NASA TECHNICAL MEMORANDUM

NASA TM X-2433

NASA TM X-2433

TOLERANCE OF MACH 2.50 AXISYMMETRIC MIXED-COMPRESSION INLETS TO UPSTREAM FLOW VARIATIONS

by David A. Choby

Lewis Research Center

Cleveland, Ohio 44135

NATIONAL AERONAUTICS AND SPACE ADMINISTRATION • WASHINGTON, D. C. • JANUARY 1972

1. Report No.	2. Government Accession No.	3. Recipient's Catalog No.
NASA TM X-2433		

4. Title and Subtitle	5. Report Date
TOLERANCE OF MACH 2.50 AXISYMMETRIC MIXED-COMPRESSION INLETS TO UPSTREAM FLOW VARIATIONS	January 1972
	6. Performing Organization Code
7. Author(s)	8. Performing Organization Report No.
David A. Choby	E-6452
	10. Work Unit No.
9. Performing Organization Name and Address	764-74
Lewis Research Center National Aeronautics and Space Administration Cleveland, Ohio 44135	11. Contract or Grant No.
	13. Type of Report and Period Covered
12. Sponsoring Agency Name and Address	Technical Memorandum
National Aeronautics and Space Administration Washington, D.C. 20546	14. Sponsoring Agency Code

15. Supplementary Notes

16. Abstract

An investigation of the tolerances of two Mach 2.50 axisymmetric mixed-compression inlets to upstream flow variations has been conducted. Tolerances of each inlet to angle of attack as a function of decreasing free-stream Mach number were obtained. A local region of overcompression was formed on the leeward side of the inlet at maximum angle of attack before unstart. This region of overcompression corresponded to local subsonic flow conditions ahead of the geometric throat. A uniform Mach number gradient of 0.10 at the cowl lip plane did not affect the inlet's pressure recovery, mass flow ratio, or diffuser exit total-pressure distortion.

17. Key Words (Suggested by Author(s))	18. Distribution Statement
Angle of attack Supersonic inlet Mixed compression inlet	Unclassified - unlimited

19. Security Classif. (of this report)	20. Security Classif. (of this page)	21. No. of Pages	22. Price*
Unclassified	Unclassified	51	$3.00

* For sale by the National Technical Information Service, Springfield, Virginia 22151

TOLERANCE OF MACH 2.50 AXISYMMETRIC MIXED-COMPRESSION INLETS TO UPSTREAM FLOW VARIATIONS

by David A. Choby

Lewis Research Center

SUMMARY

An investigation of the tolerances of two Mach 2.50 axisymmetric mixed-compression inlets to upstream flow variations has been conducted in the Lewis 10- by 10-Foot Supersonic Wind Tunnel. These variations included reductions in free-stream Mach number and a uniform Mach number gradient of 0.10 across the cowl lip plane.

Tolerances to angles of attack as a function of decreasing free-stream Mach number were obtained for the two inlets, each with two different bleed configurations. Data showed a local region of overcompression was formed on the leeward side of the inlet at maximum angle of attack before inlet unstart. This region of overcompression caused the flow to reach subsonic conditions locally ahead of the geometric throat. The flow on the windward side of the inlet appeared well behaved. By increasing or relocating the inlet bleed further upstream in the region of overcompression, larger angles of attack before unstart were obtained. A region of overcompression forward of the throat was also observed at the minimum free-stream Mach number at which the inlet would operate just prior to inlet unstart with the centerbody at the design position. In this case, the region of overcompression circumferentially encompassed the entire inlet. When a bleed change was made such that the angle-of-attack tolerance of the inlet was increased, the tolerance to Mach number reduction was also increased. A uniform Mach number gradient of 0.10 across the inlet cowl lip plane did not affect the inlet's total-pressure recovery, mass flow ratio, or diffuser exit distortion.

INTRODUCTION

In order to achieve high inlet performance and low inlet drag at cruise Mach numbers greater than 2.0, it becomes essential that some portion of the supersonic area contraction occur internally. While an inlet which utilizes a mixture of external and

internal contraction can be designed to yield the desired performance and drag characteristics, this type of inlet has an undesirable transient characteristic known as unstart which occurs when the terminal shock is forced forward of the aerodynamic throat. The unstart causes a sharp reduction in inlet total-pressure recovery and mass flow ratio. Reference 1 shows that the unstart transient can be violent enough to cause compressor stall. Studies (ref. 2) have been completed using a throat bypass which allows the inlet to absorb large internal transients without unstarting.

However, not all unstarts are caused by internal disturbances. External upstream disturbances causing changes in free-stream Mach number and angle of attack can also induce inlet unstarts. In addition the inlet flow field may be distorted by the airframe flow field. To date, very little information has been published specifically concerned with the tolerances of axisymmetric mixed-compression inlets to angles of attack or to Mach number reductions. Since the flight environment of a supersonic cruise aircraft includes gusts and thermal gradients which eventually show up as angle of attack and/or Mach number changes, a certain tolerance to these disturbances must be present in the inlet.

In order to better understand just what affect these disturbances have on the inlet and what can be done to make the inlet more tolerant to these disturbances, the present investigation was undertaken. Two high-performance Mach 2.50 axisymmetric mixed-compression inlets with different amounts of internal contraction were tested in the Lewis 10- by 10-Foot Supersonic Wind Tunnel. The testing was done at a nominal Mach number of 2.50. A flat plate was used to produce a continuous uniform Mach number reduction. Also a contoured plate was used to create a distorted flow field at the inlet cowl lip plane. Two different amounts and locations of bleed were tested in each inlet.

SYMBOLS

A	area, m^2 (ft^2)
M	Mach number
m_2/m_0	ratio of diffuser exit to free-stream capture mass flow
P	total pressure, N/m^2 (lb/ft^2)
ΔP	fluctuating component of total pressure, N/m^2 (lb/ft^2)
p	static pressure, N/m^2 (lb/ft^2)
R_C	cowl lip radius, 23.66 cm (9.315 in.)
r	local radius, cm (in.)
X	distance measured from spike tip, cm (in.)

Y thickness of plate contour (see fig. 10), cm (in.)

Z distance measured from leading edge of contoured plate, cm (in.)

α angle of attack, deg

θ_l cowl-lip-position parameter, $\tan^{-1}\left[\frac{1}{X/R_C}\right]$

ν local flow angle, deg

Subscripts:

B bottom

C cowl lip station

cp contoured plate

fp flat plate

I inlet

l local

max maximum

min minimum

rms root mean square

T top

0 free stream

2 compressor face

Superscript:

$\bar{}$ average

APPARATUS AND PROCEDURE

A complete discussion of the aerodynamic designs of both inlets tested in this investigation is presented in references 3 to 5. Both inlets were axisymmetric mixed-compression types designed to operate at Mach 2.50. Isometric views of both inlets are shown in figure 1. Throughout this report the two inlets are referred to by their percentage of external and internal area contraction. Thus the 40-60 reflecting shock inlet had 60-percent internal area contraction and is called the 40-60 inlet. The 60-40 distributed compression inlet had 40-percent internal area contraction and is called the 60-40 inlet.

The 40-60 Inlet

Figure 2 presents a detailed cross section of the model. A translating centerbody was used for starting the inlet. The 40-percent external compression was accomplished with a 12.5° half-angle conical centerbody. The 60-percent internal compression was obtained from the oblique shock generated by the 0° cowl lip and the two reflected oblique shocks plus isentropic compression between these reflected shocks.

The internal area variation from the cowl lip to the compressor face is shown in figure 3. The geometric throat was located at an X/R_C of 3.475, where the theoretical average supersonic Mach number was 1.24. At the geometric throat, the centerbody turned sharply from an angle of about 0° to -5.7°, leading to a 1° equivalent conical expansion throat region 4 hydraulic radii in length. The remainder of the subsonic diffuser was designed as an 8° equivalent conical expansion. The required subsonic diffuser length using this criterion was 3.5 cowl lip radii. However, additional length was required due to overboard bypass exit requirements. The resulting length from cone tip to compressor face was 7.86 cowl lip radii. The aft portion of the subsonic diffuser contained three hollow centerbody support struts which divided the diffuser duct into three compartments back to the compressor face. Two of these struts were used to duct centerbody bleed flow overboard.

Vortex generators were installed on the centerbody in the subsonic diffuser to prevent separation of flow from the centerbody in the bypass region when large bypass flows were discharged. Performance bleed, which consisted of porous regions on the centerbody and cowl, was located both in the supersonic diffuser and in the throat region of the inlet. The actual bleed patterns which were tested are shown in figure 4. Each of the bleed configurations removed about 5.5 percent of the total mass flow. The ejector bypass which was incorporated to provide airflow for engine cooling was sealed for this investigation.

The 60-40 Inlet

A detailed cross section of this model is presented in figure 5. A translating centerbody again was used for starting the inlet. The 60-percent external compression was accomplished with a biconical centerbody. The first and second cone half angles were 10° and 18.5°, respectively. The 40-percent internal compression was obtained from the oblique shock generated by the 5° cowl lip. Where the cowl oblique shock intersected the centerbody, the surface turned abruptly such that the shock would be theoretically canceled at that point. The cowl surface angle decreased from 5° at the lip to about 0° in the throat region. This cowl turning distributed the remaining internal compression

isentropically over a region of the centerbody which began at the cowl shock intersection point and extended a distance equal to 0.40 cowl lip radius.

The flow area variation from the cowl lip to the compressor face is shown in figure 6. The geometric throat was located at an X/R_C of 3.28, where the theoretical average supersonic Mach number was 1.30. The throat region in this inlet also had a 1° equivalent conical expansion for a length of 4 hydraulic radii. The subsonic diffuser used in this model was the same one that was used with the 40-60 inlet.

Performance bleed, consisting of regions of normal holes, was located on the cowl in the throat region and also upstream of the throat. On the centerbody, bleed was located in two regions upstream of the throat. The exact bleed patterns that were tested are shown in figure 7. Vortex generators were also installed in this model on the centerbody.

Model Instrumentation

The steady-state compressor face instrumentation, shown in figure 8, was used to determine total-pressure recovery and steady-state distortion for both inlets. This instrumentation consisted of six 10-tube total-pressure rakes and six static-pressure taps each on the cowl and centerbody. The 10-tube rakes consisted of six equal-area-weighted tubes with additional tubes added on each side of the extreme equal-area-weighted tubes in positions corresponding to an 18-tube area-weighted rake. The compressor face dynamic instrumentation, shown in figure 9, was used to measure the fluctuating component of total pressure in both inlets. Subminiature absolute pressure transducers were mounted in rakes cantilevered from the centerbody as shown in figure 9. The total-pressure transducer was mounted tangential to the tube to protect the transducer diaphragm from particle damage. The 1.905-centimeter (0.75-in.) tube length was necessary to obtain an accurate total pressure but was still short enough to yield a flat response to at least 1000 hertz. The output signals of rake transducers were filtered by first-order, low-pass filters with a 1000-hertz corner frequency and measured with trms meters.

Static-pressure taps were located in both inlets on the centerbody and cowl. The taps were in axial lines at circumferential locations of 0° and 180°. Table I gives the exact location of each tap in terms of nondimensional distance from the spike tip for each inlet.

Upstream Flow-Variation Devices

Two different devices were used to generate upstream flow variations. The first of these, shown in figure 10, was the contoured plate. The contoured plate was used to generate a Mach number and flow angle gradient such as that created by a typical airframe flow field. The second upstream flow variation device used was a flat plate. The flat plate had about the same trapezoidal shape as the contoured plate.

Figure 11 shows the installation of a Mach 2.50 inlet with the flat plate. With the inlet and flat plate both at 0° angle of attack (fig. 11(a)), the local conditions at the inlet face were not changed from the free-stream conditions. The flat plate was used to uniformly decrease free-stream Mach number so that inlet maximum angle of attack as a function of decreasing free-stream Mach number could be determined (fig. 11(b)).

The installation of a Mach 2.50 inlet with the contoured plate is shown in figure 12. The contoured plate was designed such that, when the inlet and plate were set at 0° inclination, the inlet experienced a 0.10 Mach number gradient and a 2.32° angle-of-attack gradient. The Mach number increased from 2.45 at the bottom of the inlet to 2.55 at the top of the inlet. The local flow angle that the inlet experienced varied from -1.16° at the bottom of the inlet to $+1.16^{\circ}$ at the top of the inlet. The resulting average Mach number and average angle of attack were calculated as shown in figure 12. The local flow conditions at the top and bottom of the inlet were functions of the inclination of the contoured plate and the relative positions of the inlet and contoured plate. When the contoured plate was inclined relative to the free stream, the inlet still experienced a gradient of about the same strength. However, the inlet then operated at a different average Mach number and average angle of attack. In this manner it was possible to obtain the inlet's tolerance to average angle of attack as a function of decreasing average Mach number. Figure 13 shows the 40-60 inlet and flat plate installed in the Lewis 10- by 10-Foot Supersonic Wind Tunnel.

RESULTS AND DISCUSSION

The results of this investigation are discussed in three sections. The first of these discusses the performance of the various inlets and bleed configurations at design Mach number and 0° angle of attack. The second section discusses the tolerance of the inlets to the uniform upstream variations in angle of attack and Mach number created by the flat plate. The performance of the inlets operating in the nonuniform flow fields of the contoured plate (i.e., with Mach number and angle-of-attack gradients) is presented in the third section.

Performance at Design Mach Number and 0° Angle of Attack

The 40-60 inlet. - The effect of the amount and location of porous bleed on the performance of the 40-60 inlet at 0° angle of attack is presented in figure 14. The amount of overboard bypass mass flow was 4.5 percent of capture for both bleed configurations tested. The supercritical bleed mass flow ratio was 5.5 percent for each bleed configuration. The amount and location of porous bleed area yielded no major differences in steady-state or dynamic distortion levels. The downstream bleed configuration yielded slightly higher peak pressure recovery and had more mass-flow-ratio turnover from supercritical to minimum stable operation than did the upstream bleed configuration.

Static-pressure distributions for both bleed configurations tested are presented in figures 15 and 16. Data are presented for minimum stable operation and for one or more supercritical points. The theoretical pressure distribution is shown in the figures by the dashed lines. A theoretical shock reflection point is shown as a pressure discontinuity at a point. These occur at values of X/R_C of 2.85 and 3.48 on the centerbody and 3.25 on the cowl. The experimental data show that the actual shock reflections occur upstream of the theoretical for both bleed configurations tested. A schematic of the relative shift of the experimental shock structure with respect to the theoretical is shown in figure 17. The shift in shock structure is due to the buildup of boundary layer on the cowl and centerbody surfaces. This buildup of the boundary layer and the subsequent shifting of the shocks tends to slightly overcontract the inlet.

The 60-40 inlet. - Figure 18 shows the effect of the amount and location of bleed on the performance of the 60-40 inlet. The two bleed configurations tested with this inlet are referred to as the basic and modified bleed configurations (fig. 7). The modified bleed configuration differs from the basic only in that additional bleed was incorporated on the cowl in the forward supersonic diffuser. This additional bleed reduced the supercritical mass flow ratio of the modified bleed configuration by about 1.5 percent compared to the basic bleed configuration. Both bleeds yielded about the same peak total-pressure recovery. Supercritical distortions were higher for the modified bleed configuration. Both configurations incorporated 4.5-percent overboard bypass flow.

Minimum stable and supercritical static-pressure distributions are shown for the basic and modified bleed configurations in figures 19 and 20. The theoretical static-pressure distribution is shown in the figures by the dashed lines. On the cowl, boundary-layer separation is evident at an X/R_C of 2.9 for the basic bleed configuration (fig. 19(a)). The pressure rise associated with it appears on the centerbody at an X/R_C of about 3.05 (fig. 19(b)). The added forward cowl bleed of the modified bleed configuration apparently prevented the separation at supercritical conditions (fig. 20). The pressure on the centerbody is somewhat higher than theoretical between values of X/R_C of about 2.75 to 3.00 for both configurations. The cause of the higher pressures could be

associated with partial reflection of the cowl lip oblique shock rather than with complete cancellation as designed. The reflected shock appears on the cowl at an X/R_C of 3.05 (figs. 19(a) and 20(a)) and on the centerbody at an X/R_C of 3.23 (figs. 19(b) and (20(b)). Figure 21 presents a schematic of the theoretical and experimentally determined flow fields of the 60-40 inlet.

Tolerance of Inlets to Uniform Upstream Variations in Angle of Attack and Mach Number

The 40-60 inlet. - The supercritical angle-of-attack tolerance as a function of decreasing free-stream Mach number is presented in figure 22 for the two bleed configurations tested in the 40-60 inlet. The tailed symbols denote operating points for which inlet performance data will be presented, while the solid symbols denote points for which static-pressure distributions will be presented. The data of figure 22 were obtained using the flat plate upstream of the inlet as explained in the section APPARATUS AND PROCEDURE.

The data show that the upstream bleed configuration clearly offers a greater tolerance to both angle of attack and changes in free-stream Mach number. Using the downstream bleed as a comparison, the upstream bleed doubled the Mach number tolerance but increased maximum positive angle of attack at design Mach number by only a third.

Inlet performance for limiting angles of attack at various Mach numbers (tailed symbols of fig. 22) is presented in figures 23 and 24 for the downstream and upstream bleed configurations. Inlet peak pressure recovery reached a maximum when free-stream Mach number approached a minimum (0° angle of attack). For all the data of figures 23 and 24, there was little or no mass flow turnover between supercritical and peak inlet total-pressure recovery. This indicates that, when the inlet is operating at maximum angle of attack for a given free-stream Mach number, the ability to absorb an internal flow disturbance is greatly decreased.

Static-pressure distributions for limiting angles of attack at various Mach numbers (solid symbols of fig. 22) are presented in figure 25 for the downstream bleed configuration. Two operating points are presented. The first is at design Mach number and maximum angle of attack. The second is at about 0° angle of attack and the minimum Mach number that could be obtained with a started inlet with the centerbody at the Mach 2.50 design position. Static-pressure distributions are presented for the cowl and centerbody surfaces at 0° and 180° circumferential locations. The value of static-pressure ratio which corresponds to sonic conditions is a function of free-stream Mach number and is shown on each figure. Also the location of each row of bleed holes is indicated by a tick

mark on the abscissa of the graph. The theoretical pressure distribution for the design Mach number of 2.50 and 0° angle of attack is also presented for comparison.

The most significant effect of going to angle of attack on inlet static-pressure distributions is seen on the leeward side of the inlet. Here static pressures reach values corresponding to subsonic flow conditions well ahead of the geometric throat. The theoretical pressure distributions for design Mach number and 0° angle of attack show a single sharp pressure rise on the cowl forward of the throat, indicating one shock reflection point. The angle-of-attack data (fig. 25(a)) show two such points, indicating two shock reflection points on the cowl surface. The impingement point on the centerbody of the cowl-lip-generated oblique shock has shifted forward as shown by the data of figure 25(b), at least on the leeward (top side at positive angle of attack) side of the inlet. It appears that the entire shock structure on the leeward side of the inlet is compressed and shifted upstream in the inlet, with additional shock reflections occuring upstream of the geometric throat. These additional shock reflections decelerate the flow to subsonic speeds ahead of the geometric throat. The flow then accelerates and is again supersonic when it reaches the inlet geometric throat.

The windward (bottom of inlet at positive angle of attack) side of the inlet shows no overcompression, in contrast to the leeward side. Except for the cowl-lip-generated oblique shock falling downstream of the theoretical impingement point, the data on the windward side compare well with the theoretical. Thus from the data of figure 25 it would appear that the maximum angle of attack is limited by the overcompression which occurs locally on the leeward side of the inlet. Since pressure distributions were obtained at only two circumferential locations (0° and 180°), there is no way of telling how much of the inlet was encompassed by the region of overcompression.

When an inlet is operating at angle of attack, the flow on the leeward side of the inlet sees a relatively smaller cone angle, while the flow approaching the windward side sees a steeper cone angle. This would mean that the average cowl lip Mach number would be higher on the leeward side than on the windward side. Based on only this, it would be logical that the windward side of the inlet would be overcontracted, causing unstart. However, the data show that just the opposite occurs. This contradiction can be explained by considering the flow field about the centerbody at angle of attack.

At positive angle of attack a circumferential pressure gradient exists on the forward portion of the centerbody, with the highest pressure being on the bottom. This pressure gradient produces a velocity component in the circumferential direction from the bottom to the top of the centerbody. This circumferential component of velocity will, in general, cause the flow to migrate toward the leeward side of the centerbody. The flow which will be turned the most by the circumferential velocity component is the flow in the boundary layer which has low axial velocity.

Data from a current test are presented in figure 26 to show the effect of angle of attack on boundary-layer thickness. The data shown were obtained on the leeward side of the 40-60 inlet at 2.7° angle of attack. The data were obtained at an axial location X/R_C of 2.73, which is well ahead of the first bleed region and ahead of the first cowl oblique shock reflection point. As can be seen from the data, the boundary layer has almost doubled in thickness at this point. Due to the migration of the flow field in general and the boundary layer in particular, the top (leeward side at positive angle of attack) of the inlet tends to overcontract. This overcontraction limits the maximum angle of attack attainable before inlet unstart.

Figures 25(c) and (d) present additional data obtained with the downstream bleed configuration in the 40-60 inlet. The data are for the inlet operating at about 0° angle of attack at the minimum free-stream Mach number at which the inlet would remain started (Mach 2.414). For this case the inlet was uniformly overcontracted, as shown by the symmetry of the data obtained at circumferential locations of 0° and 180°. The overcompression at both of these locations is similar to that which occurred on the leeward side of the inlet at maximum angle of attack. It would appear that the inlet, for a given bleed configuration, is sensitive to a given magnitude of overcompression in terms of static-pressure ratio. Further, it does not seem to make any difference whether the overcompression is circumferentially local (design Mach number, maximum angle of attack) or encompasses the entire inlet (minimum Mach number, 0° angle of attack).

It would seem that additional angle-of-attack and Mach number tolerance could be obtained by a more forward location of the porous bleed. The second bleed configuration tested with the 40-60 inlet incorporated most of the porous bleed area in the regions of the cowl and centerbody where the maximum overcompression occurred resulting in subsonic flow. As was previously shown (fig. 22) this bleed configuration (upstream bleed) increased both angle-of-attack and Mach number tolerance.

Static-pressure distributions are presented in figure 27 for the upstream bleed configuration. Figures 27(a) and (b) are for the inlet operating at design Mach number and maximum angle of attack. Figures 27(c) and (d) were obtained with the inlet very near to 0° angle of attack and at the minimum Mach number attainable. The data of figure 27 are similar to those of figure 25. The shock reflections appear to have shifted upstream slightly more. Figure 28 presents a schematic representation of the experimentally determined shock structures at design Mach number in the 40-60 inlet for 0° angle of attack and for the maximum angles of attack obtained with the two bleed configurations tested. The shock structures shown were those formed on the leeward side of the inlet.

The 60-40 inlet. - Data were also obtained which determined the tolerance of the 60-40 inlet to angle of attack as a function of free-stream Mach number. These data, shown in figure 29, were obtained using the flat plate to obtain uniform variations in Mach number and angle of attack. As seen from the figure the maximum angles of attack that were

attained by the 60-40 inlet were greater than those attained by the 40-60 inlet (fig. 22). The maximum tolerance to a reduction in free-stream Mach number was about the same for both inlets. Static-pressure distributions were not obtained when the 60-40 inlet was run with the flat plate. However, static-pressure distributions were obtained when the 60-40 inlet was run with the contoured plate and are presented in a following section.

Tolerance of Inlets to Nonuniform Upstream Variations in Angle of Attack and Mach Number

The 40-60 inlet. - The effect of a Mach number and angle-of-attack gradient on inlet performance is shown in figure 30. These gradients were produced with the contoured plate that was described in the section APPARATUS AND PROCEDURE. This contoured plate caused a gradient in angle of attack of 2.32°, varying from -1.16° at the bottom of the inlet to $+1.16^{\circ}$ at the top of the inlet. The accompanying Mach number gradient was 0.10, with an average Mach number of 2.496. As can be seen in figure 30, the mass flow pressure recovery and distortion characteristics of the inlet were not affected by the presence of the gradient. These data were obtained with the 40-60 inlet tested with the upstream bleed configuration. The effect of the gradient on internal static-pressure distributions is shown in figure 31. The data presented are for a supercritical operating point with and without the gradient imposed upon the inlet. Data are presented for two circumferential locations, 0° and 180°, for both the cowl and centerbody surfaces. These data show the gradient did not significantly affect the pressure distributions on the cowl or centerbody. Similar data were obtained for the 40-60 inlet with the downstream bleed and also for the 60-40 distributed compression inlet with both bleed configurations that were tested. In each case the results were similar to the results presented in figures 30 and 31; that is, the Mach number and angle-of-attack gradient for the two configurations tested with each inlet had no effect on inlet performance.

The effect of angle-of-attack and Mach number gradients on the tolerance of the 40-60 inlet to average angle of attack as a function of average free-stream Mach number is shown in figure 32. The inlet's tolerance to angle of attack as a function of Mach number for uniform flow field conditions is also shown for comparative purposes. The data were plotted for the average Mach number and average angle of attack that the inlet experiences. The results obtained with the downstream bleed are presented in figure 32(a). The effect of the flow field gradient tends to be slight at positive average angles of attack. The reason for this can be explained by observing the nature of the gradient. At positive angles-of-attack the gradient tends to locally increase angle of attack and Mach number on the leeward (top) side of the inlet. These two effects tend to cancel since increasing

Mach number increases angle-of-attack tolerance. However, at negative average angles of attack the gradient increases the absolute value of local angle of attack (a greater negative angle of attack occurs locally) and decreases Mach number on the leeward (bottom) side of the inlet. The net result is that for a given average Mach number the tolerance to average angle of attack is decreased. The data obtained with the upstream bleed configuration (fig. 32(b)) follow the same trend with some scatter in the positive angle-of-attack data.

Schlieren photographs of the external shock structure of the 40-60 inlet are shown in figure 33. The symmetric shock pattern corresponding to design Mach number and 0° angle of attack is shown in figure 33(a). Figure 33(b) shows the inlet operating at maximum angle of attack with the initial cone shock being unsymmetrically displaced from the cowl lip. The minimum Mach number condition attainable at about 0° angle of attack is shown in figure 33(c). In this case the shocks fall uniformly outside of the cowl lip because of the reduced free-stream Mach number. Figure 33(d) to (f) were obtained with the gradient imposed upon the inlet. When the average angle of attack is 0° and the average Mach number is equal to design, the shock structure is unsymmetrical due to the gradient. Similar effects can be seen in figures 33(e) and (f).

The 60-40 inlet. - Angle-of-attack tolerance as a function of free-stream Mach number is shown in figure 34 for the 60-40 inlet. Data are presented with the inlet operating in the Mach number - angle-of-attack flow field gradient. Inlet performance data will be presented for the operating conditions indicated by the tailed symbols. Static-pressure distributions will be presented for the operating points indicated by the solid symbols. Both the basic and modified bleed configurations of the 60-40 inlet offered greater angle-of-attack tolerance than did the 40-60 inlet. However, the 60-40 inlet with the basic bleed (no forward cowl bleed) offered very little tolerance to decreases in free-stream Mach number. Since very few data were obtained with this inlet at positive angles of attack with a uniform flow field, it is not possible to see the effect of the gradient at positive angles of attack. The 60-40 inlet had slightly more Mach number tolerance when operating in the gradient. The decreased average negative angle-of-attack tolerance was again observed when the inlet was operated with the gradient, especially when the basic bleed configuration was tested.

Figures 35 and 36 present inlet performance for the inlet operating at the various conditions shown in figure 34. The performance data were obtained with the inlet operating in the flow field gradient. As was noticed with the 40-60 inlet, all mass-flow-ratio turnover between supercritical and minimum stable was lost when the 60-40 inlet was operated at maximum average angle-of-attack conditions. Because the 60-40 inlet could operate at higher angles of attack at design Mach number, the inlet total-pressure distortions were higher. Distortion, however, decreased when the inlet was operated at low angles of attack near the minimum free-stream Mach number attainable. The higher distortions at large angles of attack were primarily circumferential.

Static-pressure distributions for the 60-40 inlet with the basic and modified bleed configurations are presented in figures 37 and 38, respectively. For each bleed configuration, two operating conditions are shown. The first is near maximum angle of attack and design Mach number, the second is at low angle of attack near minimum free-stream Mach number (solid symbols shown in fig. 34).

The trend of the data obtained with the 60-40 inlet was similar to that obtained with the 40-60 inlet. At large angles of attack near design Mach number (figs. 37(a) and 38(a)), the leeward side of the inlet showed evidence of local overcompression of the flow. With the basic bleed configuration, the flow did not reach subsonic conditions ahead of the throat at maximum angle of attack at design Mach number. This was the only bleed configuration tested (for either inlet) where local subsonic flow did not occur ahead of the throat at maximum angle of attack or at minimum attainable free-stream Mach number conditions. This bleed configuration also had the least amount of tolerance to decreases in free-stream Mach number. This configuration may be sensitive to decreasing Mach number due to the flow separation on the cowl (fig. 19(a)). With additional forward cowl bleed (modified bleed) the maximum angle-of-attack tolerance at design Mach number was increased from 4.5° (basic bleed configuration) to 7.5°. The tolerance to decreases in free-stream Mach number for the modified bleed configuration was comparable to the better 40-60 bleed configuration tested; that is, a decrease in Mach number from design of about 0.14 was attained.

SUMMARY OF RESULTS

An investigation of the tolerance of Mach 2.5 axisymmetric mixed-compression inlets to upstream flow variations has been conducted in the 10- by 10-Foot Supersonic Wind Tunnel. The test was conducted at Mach numbers of 2.34 to 2.50 with the following results:

1. Maximum inlet supercritical angle of attack is limited by inlet unstart, which is caused by local overcompression on the leeward side of the inlet. This region of overcompression caused subsonic flow ahead of the geometric throat in three of four bleed configurations tested in two different inlets.

2. Higher angles of attack before unstart were obtained when porous bleed areas were located farther upstream of the throat. This permitted the overcompression regions to move farther upstream in the inlet. The overcompression to Mach 1.0 or below could not be obtained upstream of a bleed region.

3. At maximum angle of attack at design Mach number the flow appeared well behaved on the windward side of the inlet.

4. When operating at 0° angle of attack and at the minimum Mach number attainable before unstart, overcompression similar to that obtained at maximum angle of attack again appeared forward of the throat and circumferentially encompassed the entire inlet flow field.

5. The maximum attainable tolerance to decreases in free-stream Mach number was similar for both inlets. However, the inlet having the greater amount of external area contraction exhibited greater tolerance to angle of attack.

6. A flow field distortion consisting of a 0.10 Mach number gradient and a 2.3° angle-of-attack gradient had no significant affect on inlet performance.

Lewis Research Center,
National Aeronautics and Space Administration,
Cleveland, Ohio, July 29, 1971,
764-74.

REFERENCES

1. Choby, David A.; Burstadt, Paul L.; and Calogeras, James E.: Unstart and Stall Interactions Between a Turbojet Engine and an Axisymmetric Inlet With 60-Percent Internal-Area Contraction. NASA TM X-2192, 1971.

2. Sanders, Bobby W.; and Mitchell, Glenn A.: Increasing the Stable Operating Range of a Mach 2.5 Inlet. Paper 70-686, AIAA, June 1970.

3. Cubbison, Robert W.; Meleason, Edward T.; and Johnson, David F.: Effect of Porous Bleed in a High-Performance Axisymmetric, Mixed-Compression Inlet at Mach 2.50. NASA TM X-1692, 1968.

4. Cubbison, Robert W.; Meleason, Edward T.; and Johnson, David F.: Performance Characteristics From Mach 2.58 to 1.98 of an Axisymmetric Mixed-Compression Inlet System With 60-Percent Internal Contraction. NASA TM X-1739, 1969.

5. Wasserbauer, Joseph F.; and Choby, David A.: Performance of a Mach 2.5 Bicone Inlet With Internal Distributed Compression and 40-Percent Internal Contraction. NASA TM X-2416, 1971.

TABLE I. - LOCATION OF INTERNAL STATIC-PRESSURE TAPS IN INLET MODELS, X/R_C

40-60 Inlet				60-40 Inlet			
Cowl		Centerbody		Cowl		Centerbody	
Top (0^o)	Bottom (180^o)	Top (0^o)	Bottom (180^o)	Top (0^o)	Bottom (180^o)	Top (0^o)	Bottom (180^o)
2.82	2.82	2.36	2.36	2.68	2.68	2.60	2.60
3.13	2.87	2.82	2.79	2.81	2.81	2.67	2.67
3.24	3.12	2.93	2.81	2.89	2.89	2.72	2.72
3.30	3.14	3.04	2.83	2.93	2.93	2.75	2.75
3.38	3.16	3.31	2.86	2.96	2.96	2.78	2.78
3.43	3.18	3.44	2.88	3.00	3.00	2.80	2.80
3.49	3.20	3.54	2.90	3.04	3.04	2.83	2.83
3.53	3.21	3.66	2.92	3.07	3.07	2.86	2.86
3.57	3.23	3.76	2.94	3.10	3.10	2.89	2.89
3.61	3.25		2.96	3.14	3.14	2.96	2.96
3.64	3.26		2.98	3.17	3.17	3.03	3.03
3.68	3.28		3.16	3.21	3.21	3.10	3.10
3.72	3.30		3.18	3.24	3.24	3.14	3.14
3.75	3.32		3.20	3.28	3.28	3.17	3.17
3.86	3.36		3.22	3.31	3.31	3.21	3.21
3.96	3.38		3.24	3.35	3.35	3.25	3.25
4.12	3.40		3.26	3.38	3.38	3.29	3.29
	3.43		3.32	3.43	3.43	3.32	3.32
	3.45		3.33	3.49	3.49	3.35	3.35
	3.47		3.35	3.64	3.64	3.39	3.39
	3.49		3.37	3.68	3.68	3.44	3.44
	3.51		3.39	3.78	3.78	3.49	3.49
	3.53		3.40	3.95	3.95	3.54	3.54
	3.67		3.42			3.59	3.59
	3.72		3.44			3.63	3.63
	3.74		3.46			3.67	3.67
			3.48			3.71	3.71
			3.50			3.80	3.80
			3.52			3.88	3.88
			3.58			3.95	3.95

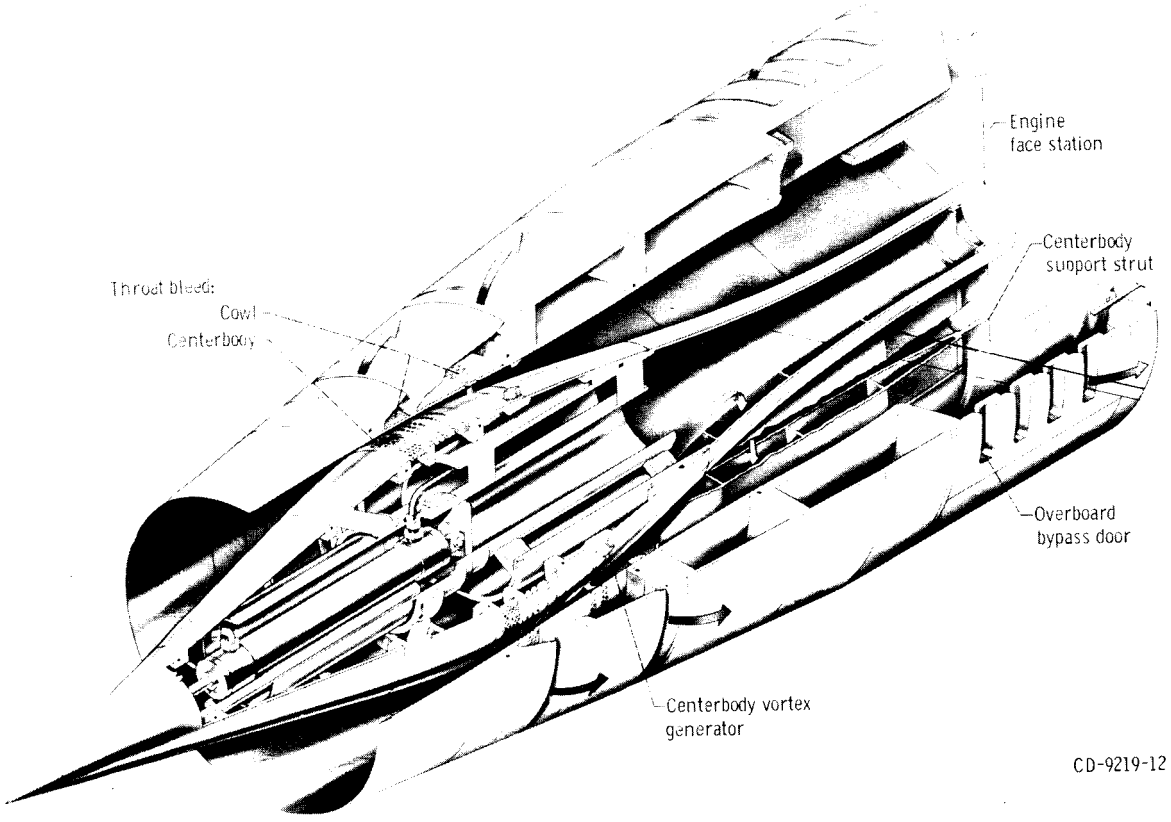

(a) Reflecting shock inlet with 60-percent internal area contraction (40 - 60 inlet).

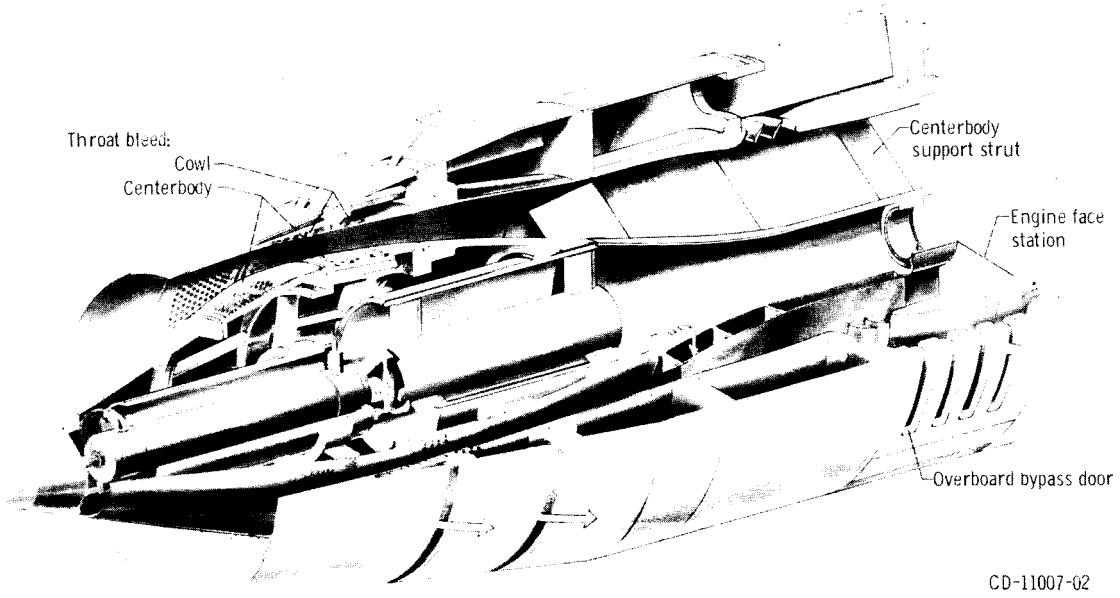

(b) Distributed compression inlet with 40-percent internal area contraction (60 - 40 inlet).

Figure 1. - Cutaway view of inlets.

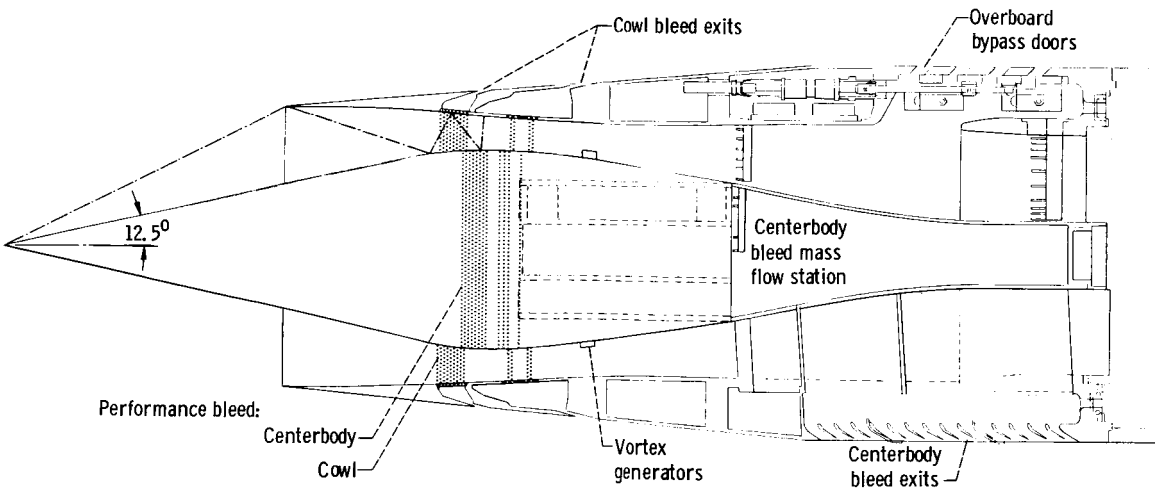

Figure 2. - Details of 40 - 60 inlet.

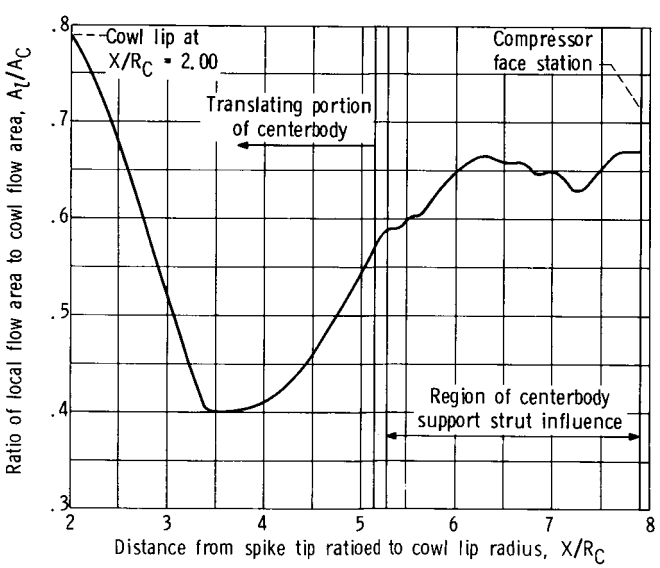

Figure 3. - Internal flow area variation of 40-60 inlet.

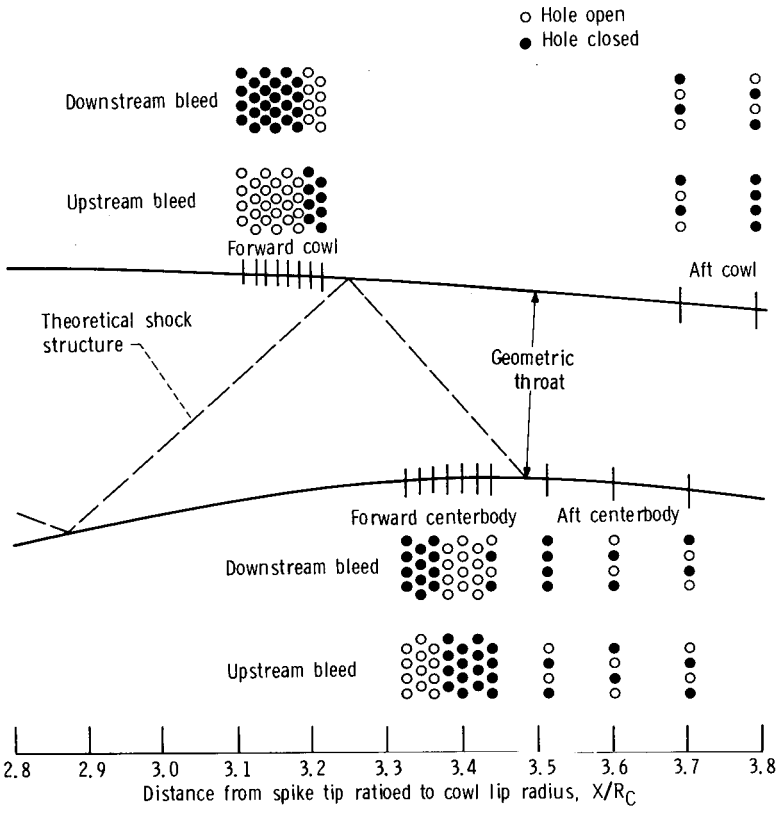

Figure 4. - Amount and location of performance bleed in 40-60 inlet. Hole diameter, 0.3175 centimeter (0.125 in.).

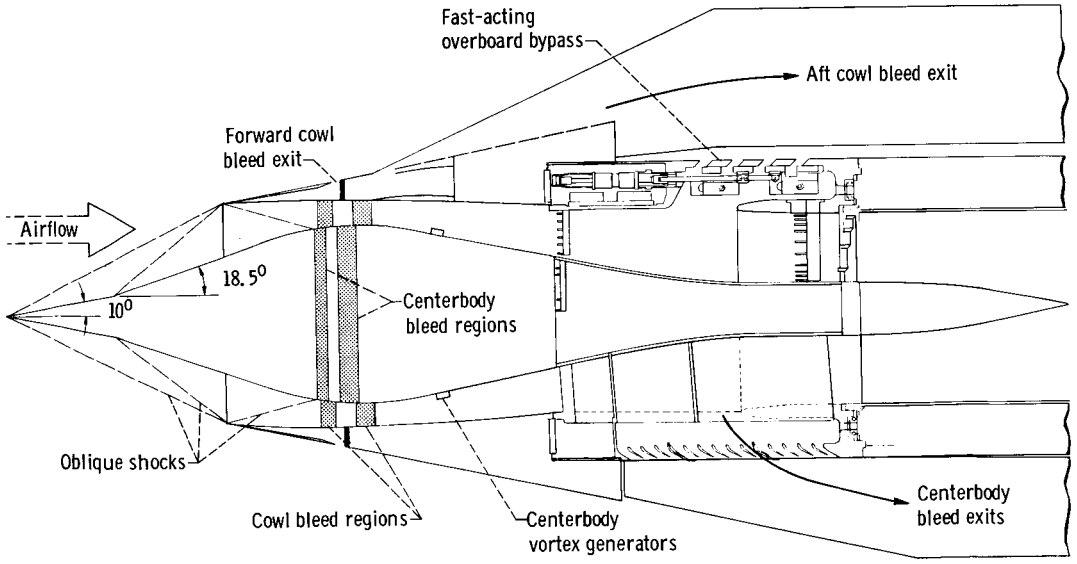

Figure 5. - Details of 60 - 40 inlet.

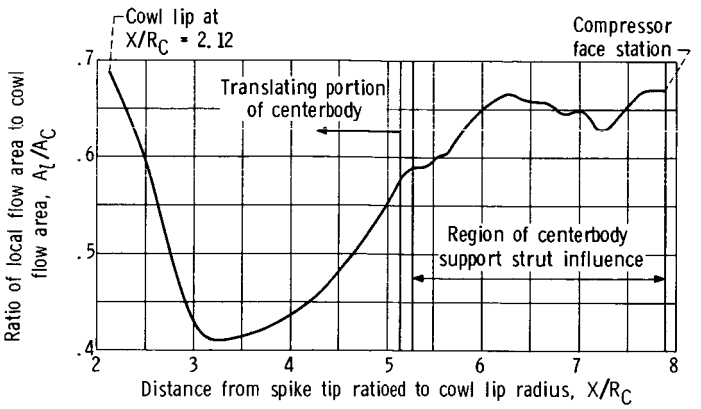

Figure 6. - Internal flow area variation of 60-40 inlet.

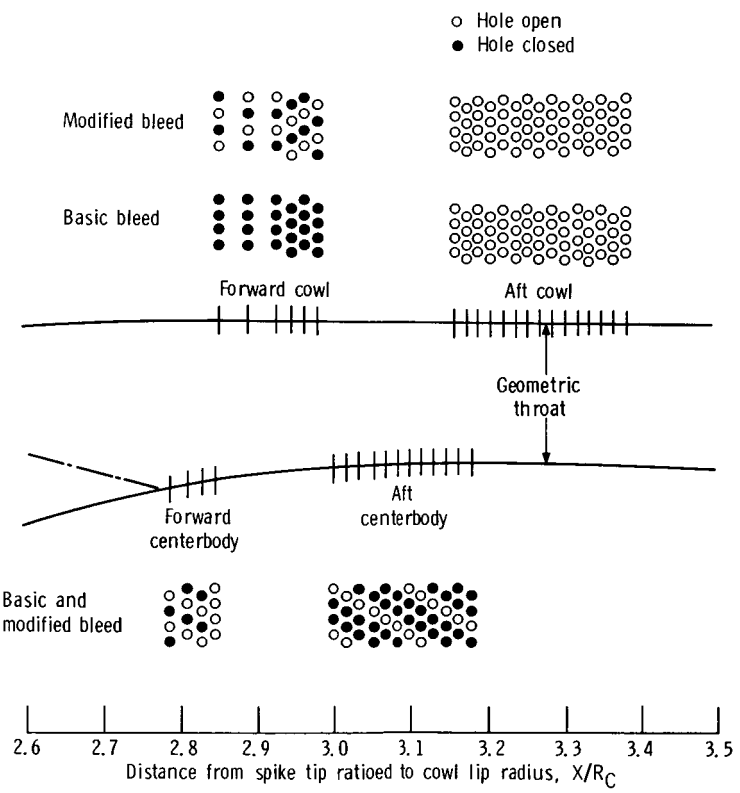

Figure 7. - Amount and location of performance bleed in 60-40 inlet. Hole diameter, 0.3175 centimeter (0.125 in.).

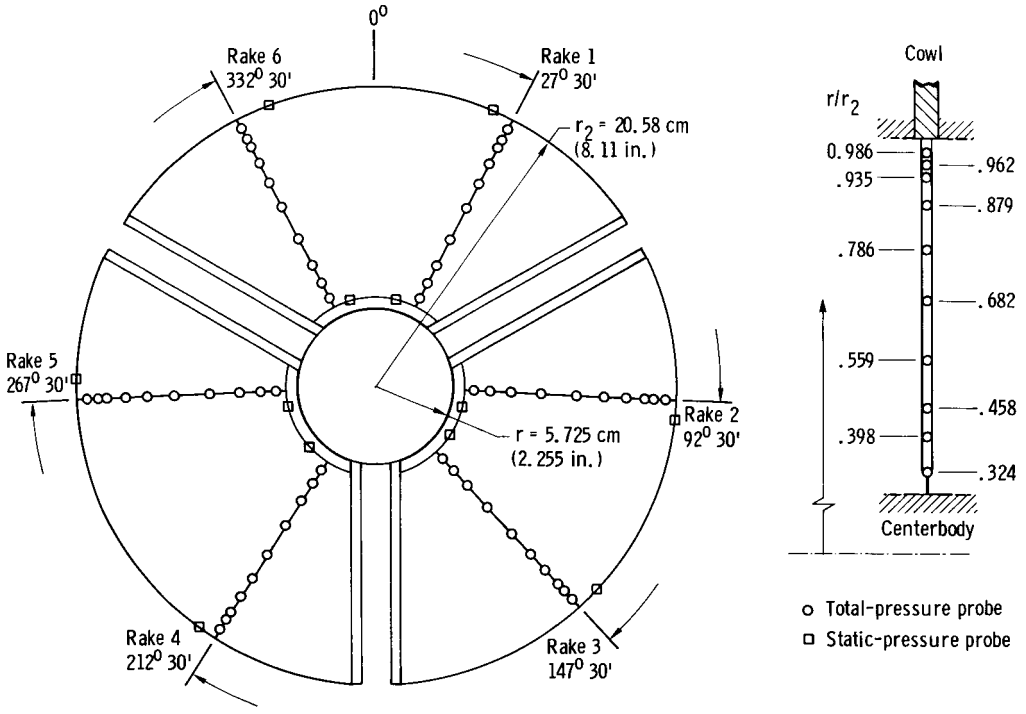

Figure 8. - Compressor face steady-state instrumentation common to both inlet models, looking downstream.

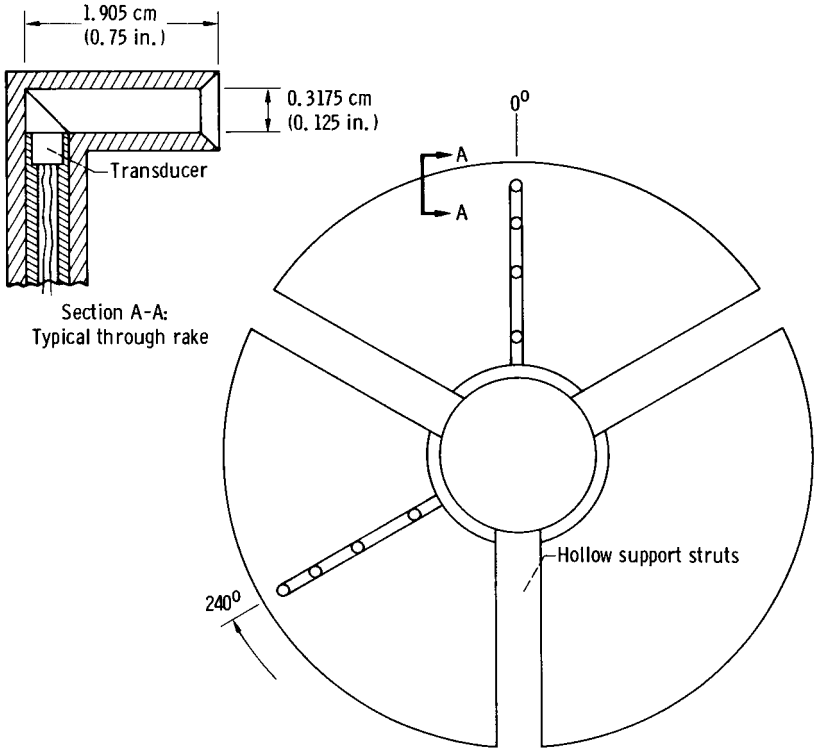

Figure 9. - Compressor face dynamic instrumentation, looking downstream.
This instrumentation is common to both inlet models.

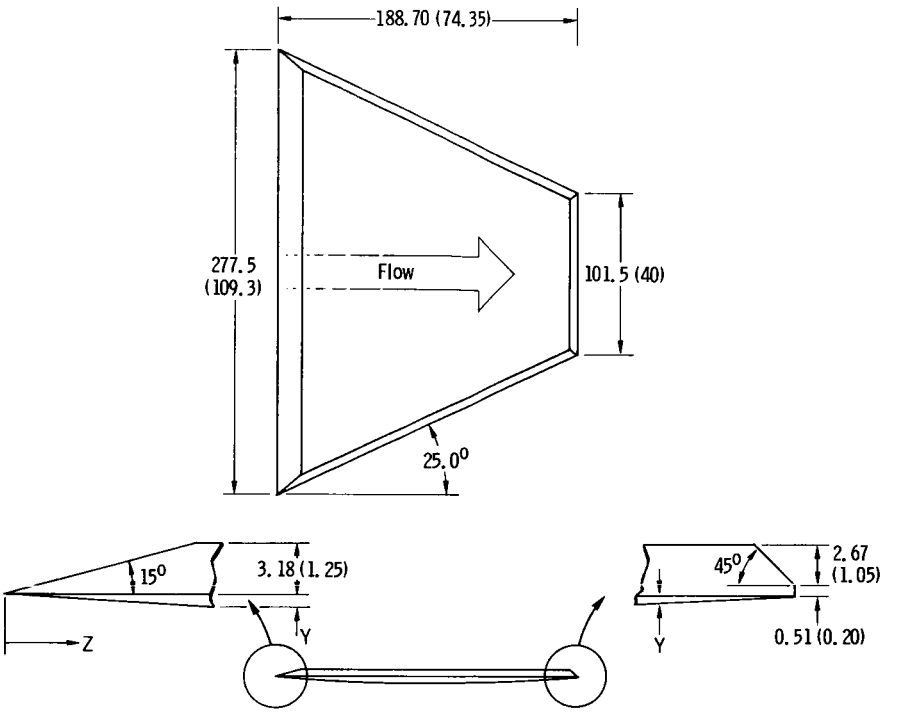

Z	Y	Z	Y
cm		in.	
0	0	0	0
25.4	.838	10.0	.330
34.6	1.100	13.6	.434
43.7	1.512	17.2	.596
52.8	1.662	20.8	.655
62.0	1.778	24.4	.699
73.1	1.850	28.8	.728
80.3	1.884	31.6	.742
89.5	1.884	35.2	.742
98.6	1.848	38.8	.727
107.7	1.772	42.4	.698
116.9	1.660	46.0	.654
125.9	1.510	49.6	.595
135.0	1.325	53.2	.522
144.2	1.105	56.8	.435
153.4	.840	60.4	.331
188.7	0	74.35	

Figure 10. - Details of contoured plate. (Dimensions are in cm (in.) unless noted.)

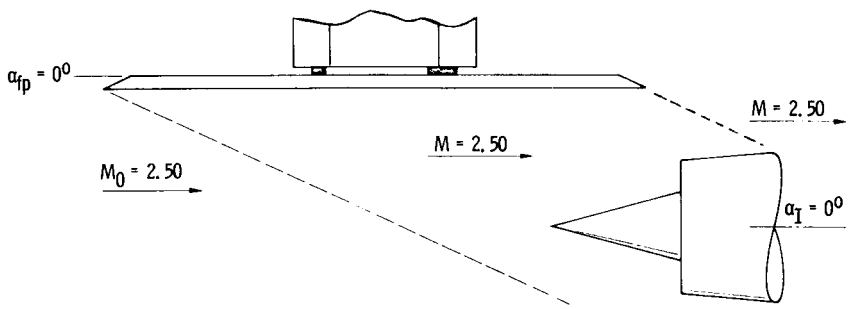

(a) Inlet operating at uniform design conditions: $M = 2.50$; $\alpha = 0^0$.

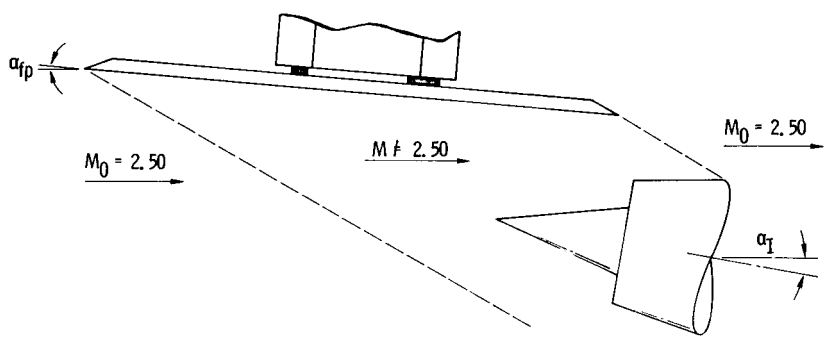

(b) Inlet operating at uniform off-design conditions: $M \neq 2.50$; $\alpha \neq 0^0$.

Figure 11. - Typical installation of Mach 2.50 inlet with flat plate, where M is function of plate angle of attack and $\alpha = \alpha_I - \alpha_{fp}$.

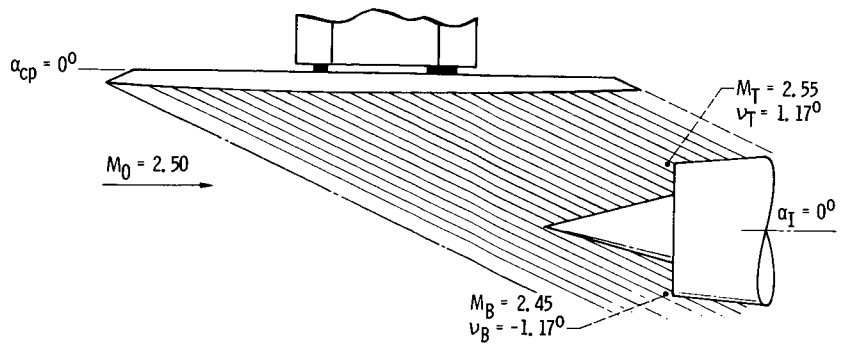

(a) Inlet operating at average design conditions: $\overline{M} = 2.50$; $\overline{\alpha} = 0^0$.

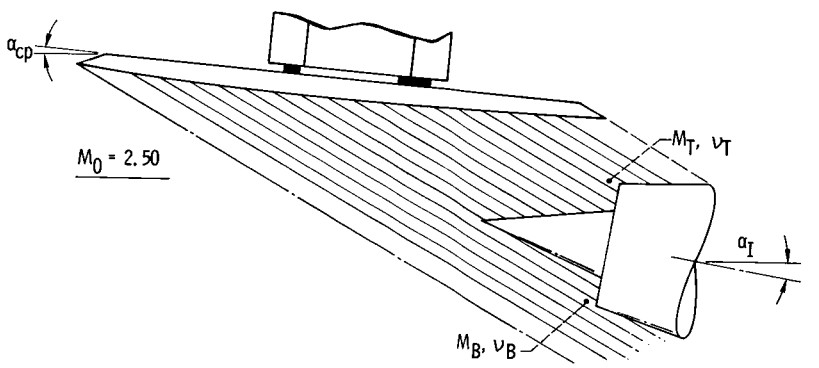

(b) Inlet operating at average off-design conditions: $\overline{M} \neq 2.50$; $\overline{\alpha} \neq 0^0$.

Figure 12. - Typical installation of Mach 2.50 inlet with contoured plate, where $\overline{M} = \frac{1}{2}(M_T + M_B)$ and $\overline{\alpha} = \alpha_I - \frac{1}{2}(\nu_T + \nu_B)$. M_T, M_B, ν_T, and ν_B are functions of plate angle of attack α_I and relative position of inlet to plate.

Figure 13. - Installation of 40-60 inlet and flat plate in 10- by 10-Foot Supersonic Wind Tunnel.

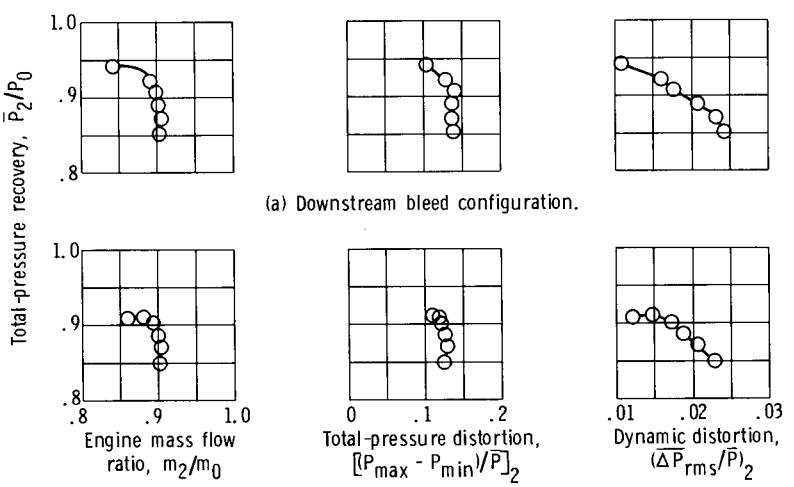

(b) Upstream bleed configuration.

Figure 14. - Effect of amount and location of porous bleed on 40-60 inlet performance at Mach 2.495 and 0^0 angle of attack. Cowl-lip-position parameter, 26.60^0.

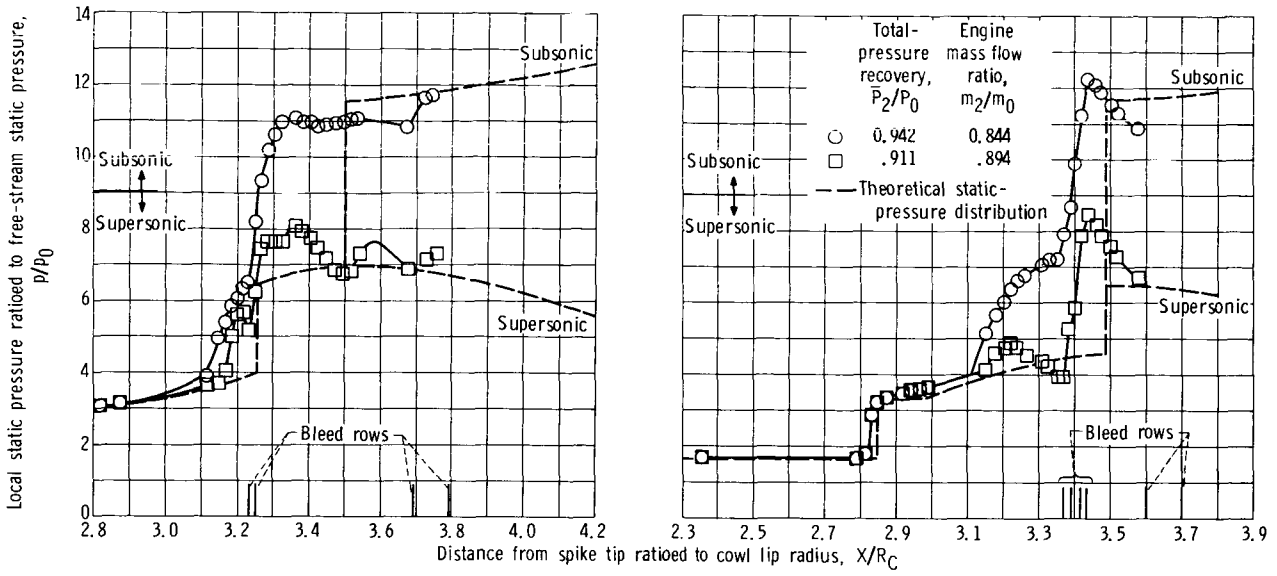

(a) Cowl surface.

(b) Centerbody surface.

Figure 15. - Static-pressure distributions of 40-60 inlet at Mach 2.496, and 0° angle of attack with downstream bleed configuration. Cowl-lip-position parameter, 26.60°.

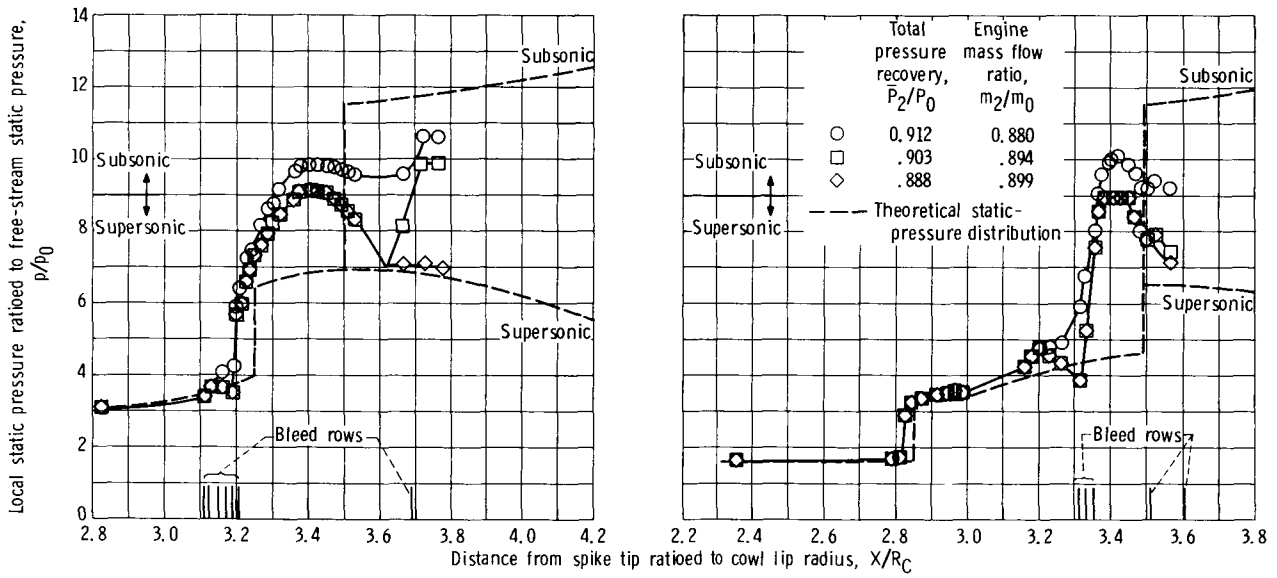

(a) Cowl surface.

(b) Centerbody surface.

Figure 16. - Static-pressure distributions of 40-60 inlet at Mach 2.496 and 0° angle of attack with upstream bleed configuration. Cowl-lip-position parameter, 26.60°.

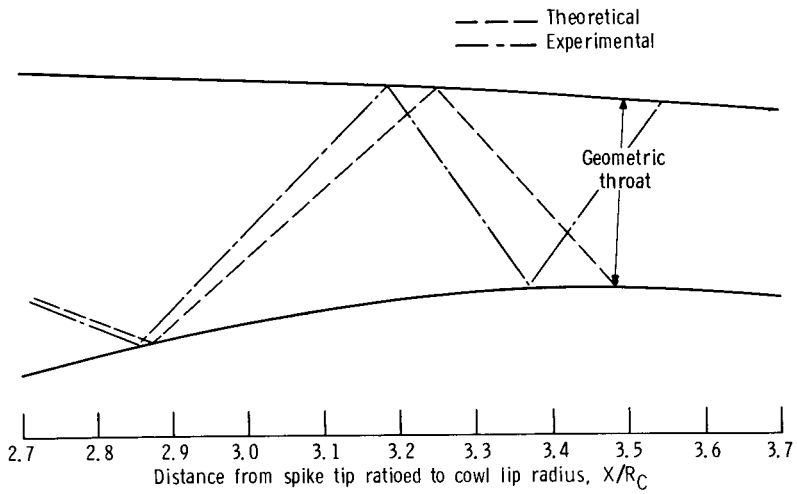

Figure 17. - Comparison of theoretical and experimental shock structures in the 40-60 inlet at Mach 2.496, 0^0 angle of attack, and supercritical operating condition.

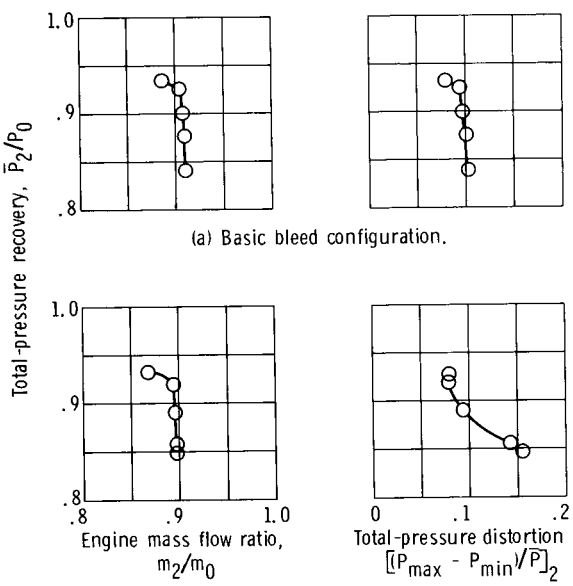

Figure 18. - Effect of amount and location of porous bleed on performance of 60-40 inlet. Cowl-lip-position parameter, 25.25^0.

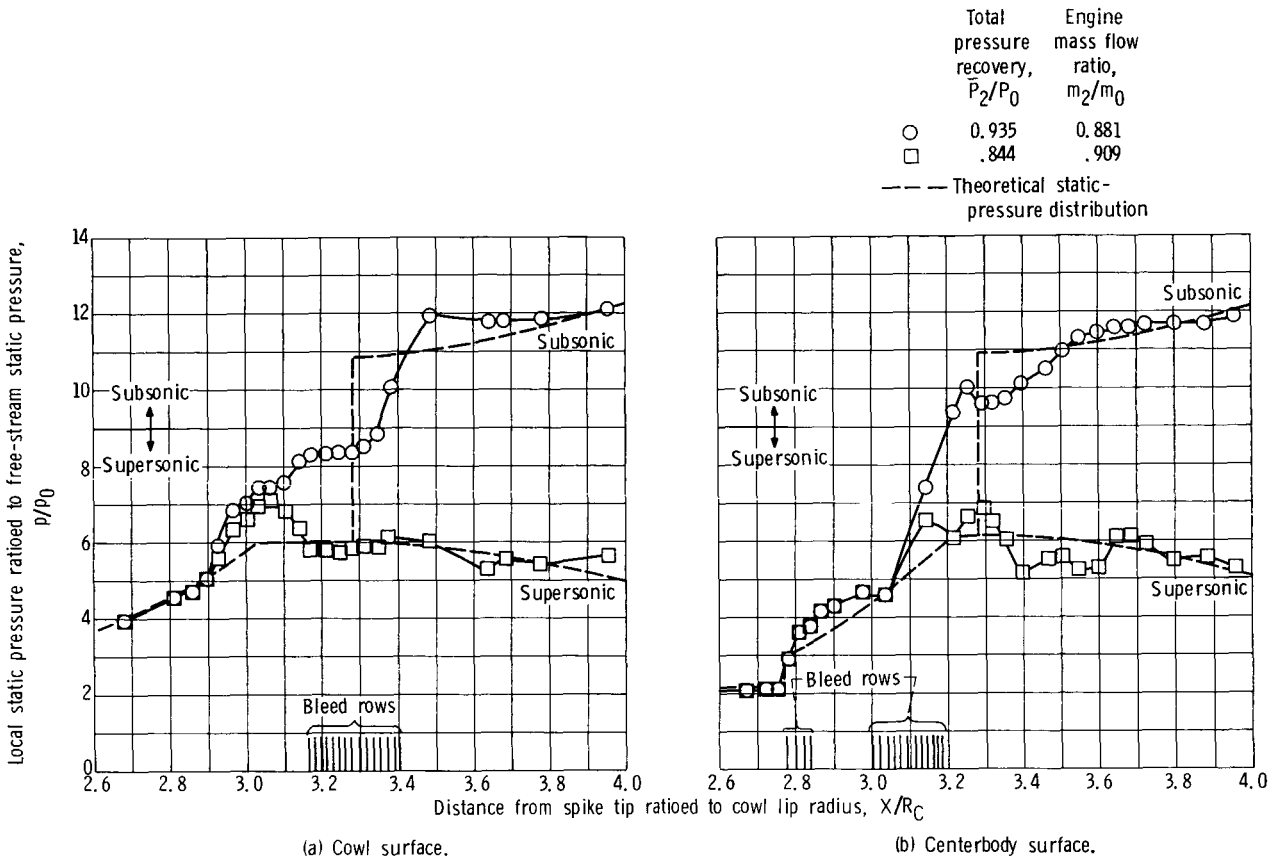

(a) Cowl surface.

(b) Centerbody surface.

Figure 19. - Static-pressure distributions of the 60-40 inlet at 0^0 angle of attack and Mach 2.496, basic bleed configuration; cowl-lip-position parameter, 25.25^0.

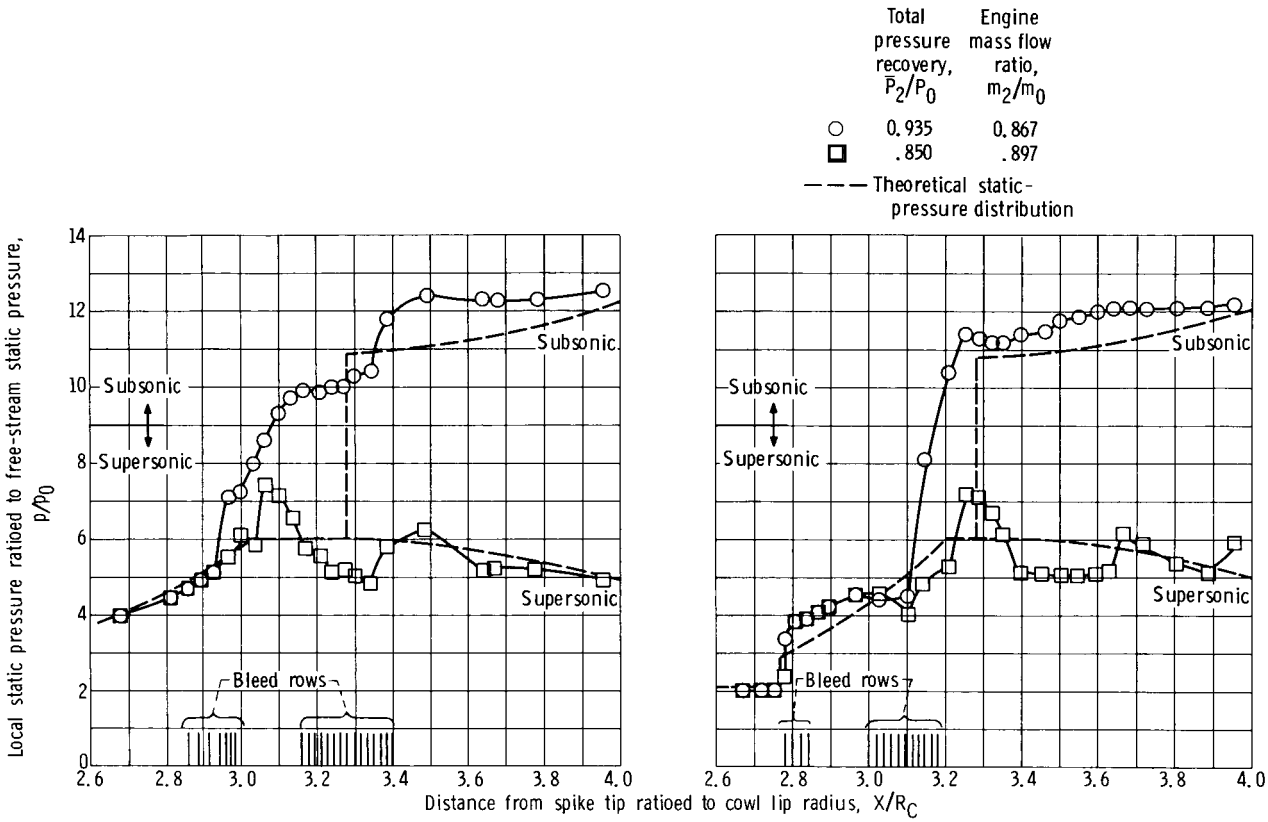

(a) Cowl surface.

(b) Centerbody surface.

Figure 20. - Static-pressure distributions of the 60-40 inlet at 0^0 angle of attack and Mach 2.496, modified bleed configuration. Cowl-lip-position parameter, 25.25^0.

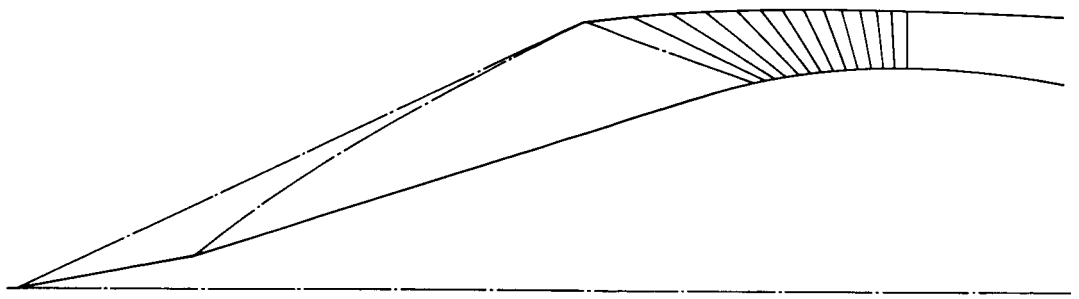

(a) Theoretical flow field; canceled shock with isentropic compression.

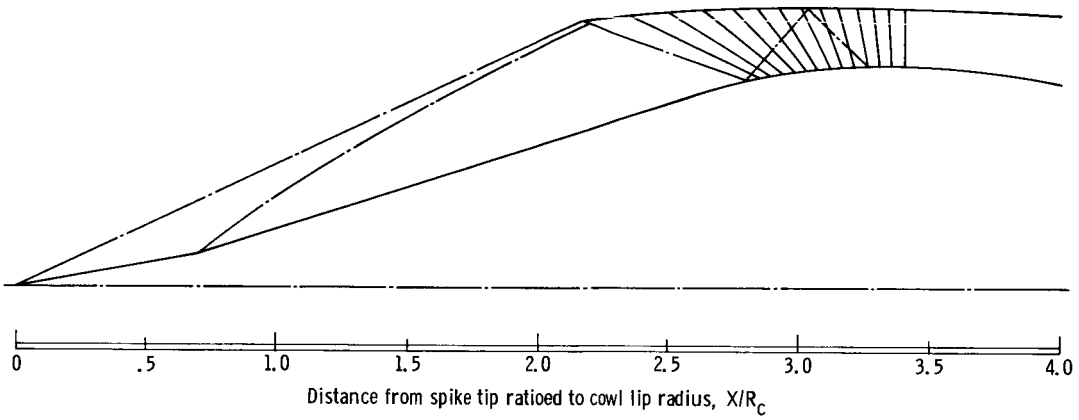

(b) Experimental flow field; reflecting shocks plus isentropic compression.

Figure 21. - Comparison of theoretical and experimentally determined flow fields in 60 - 40 inlet at supercritical operating condition.

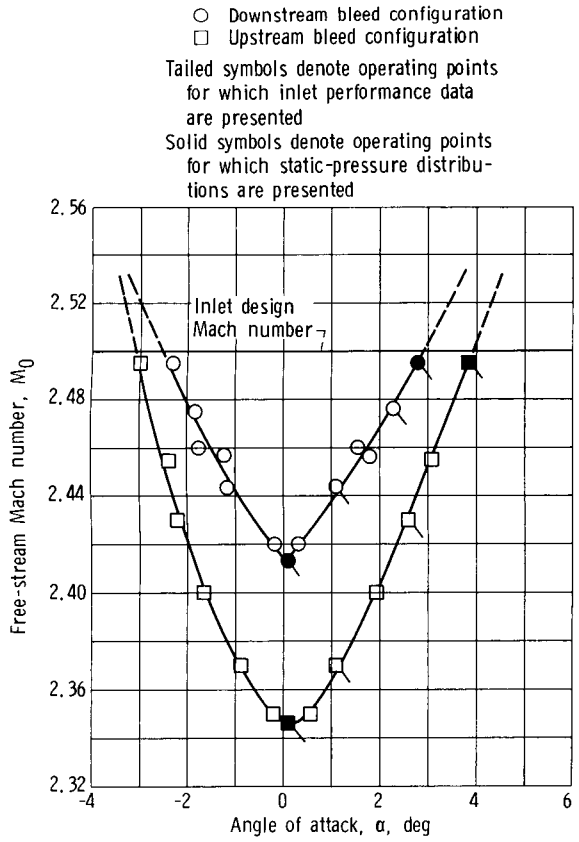

Figure 22. - Mach number - angle-of-attack tolerances of 40-60 inlet. Cowl-lip-position parameter, 26.60°.

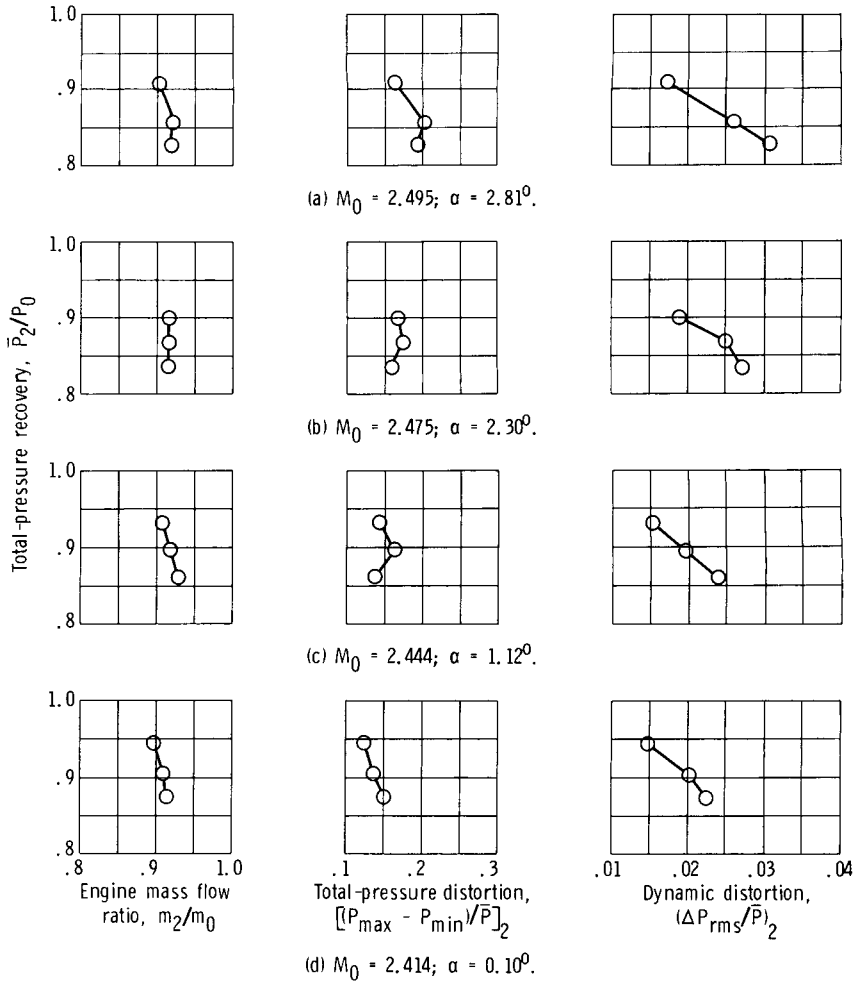

Figure 23. - Performance of 40-60 inlet at various limits for downstream bleed configuration. Cowl-lip-position parameter, 26.60°.

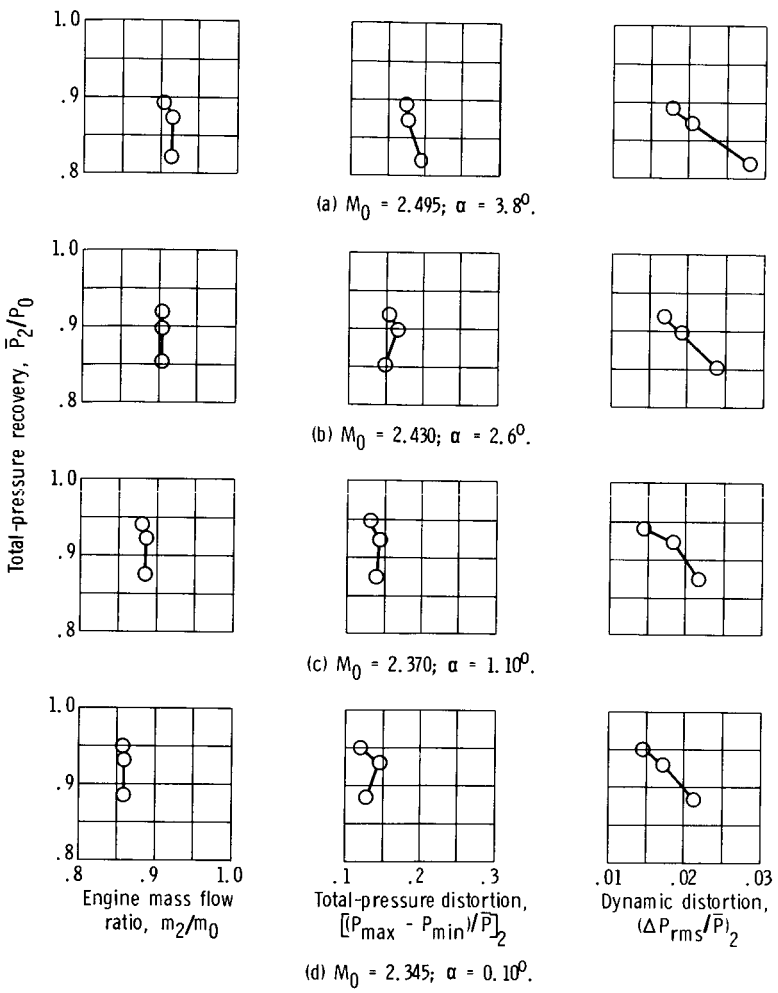

Figure 24. - Performance of 40-60 inlet at various limits for the upstream bleed configuration. Cowl-lip-position parameter, 26.60°.

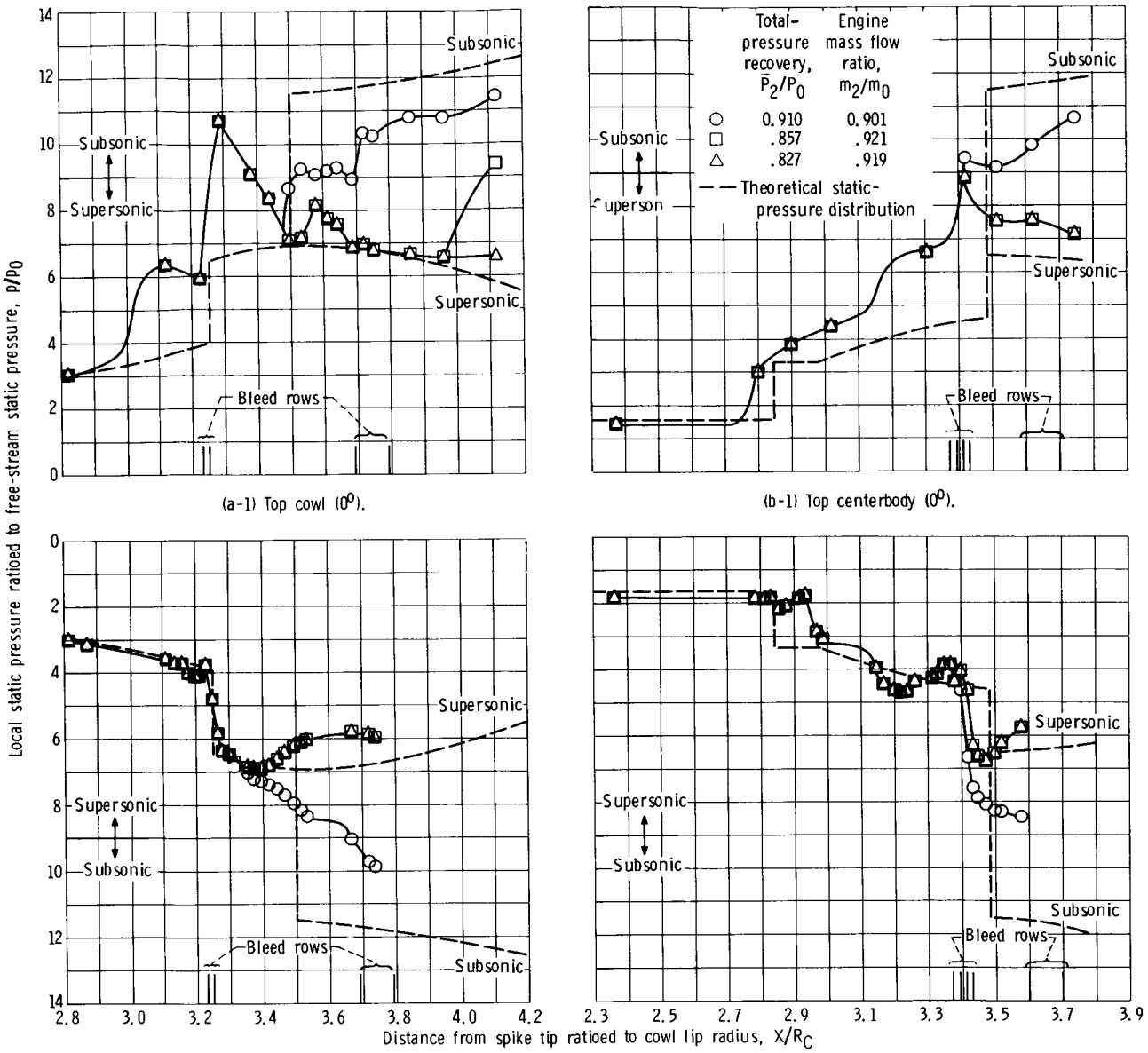

(a-1) Top cowl (0^0).

(b-1) Top centerbody (0^0).

(a-2) Bottom cowl (180^0).

(b-2) Bottom centerbody (180^0).

(a) Cowl surface; $M_0 = 2.495$; $\alpha = 2.81^0$.

(b) Centerbody surface; $M_0 = 2.495$; $\alpha = 2.81^0$.

Figure 25. - Static-pressure distributions of 40-60 inlet at various operating limits for downstream bleed configuration. Cowl-lip-position parameter, 26.60^0.

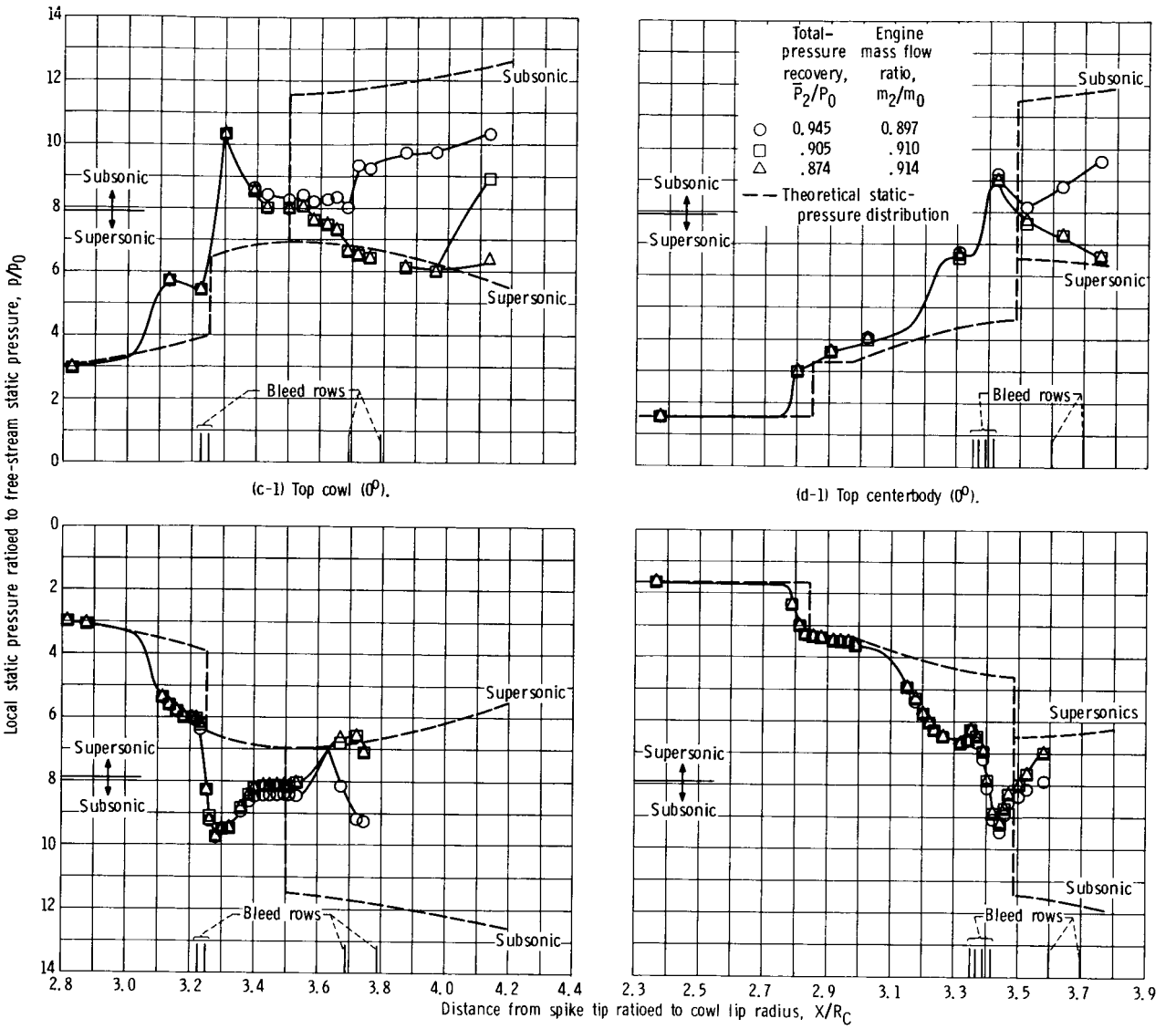

(c-1) Top cowl (0^0).

(d-1) Top centerbody (0^0).

(c-2) Bottom cowl (180^0).

(d-2) Bottom centerbody (180^0).

(c) Cowl surface; $M_0 = 2.414$; $\alpha = 0.10^0$.

(d) Centerbody surface; $M_0 = 2.414$; $\alpha = 0.10^0$.

Figure 25. - Concluded.

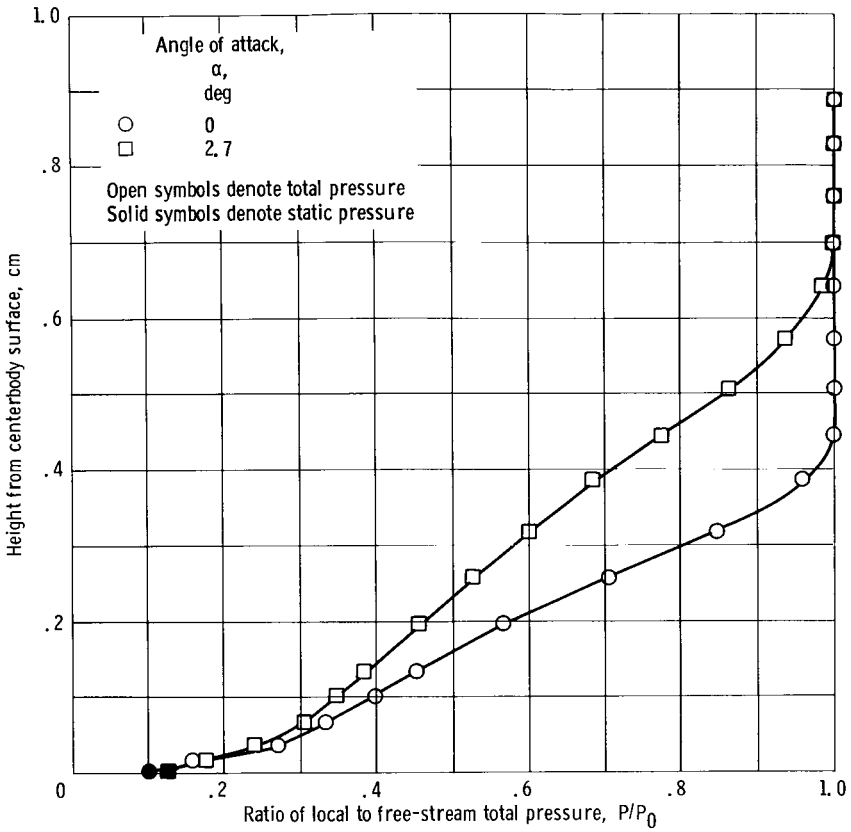

Figure 26. - Effect of angle of attack on the boundary layer on the leeward side of the 40-60 inlet at Mach 2.50. Cowl-lip-position parameter, 26.60^0.

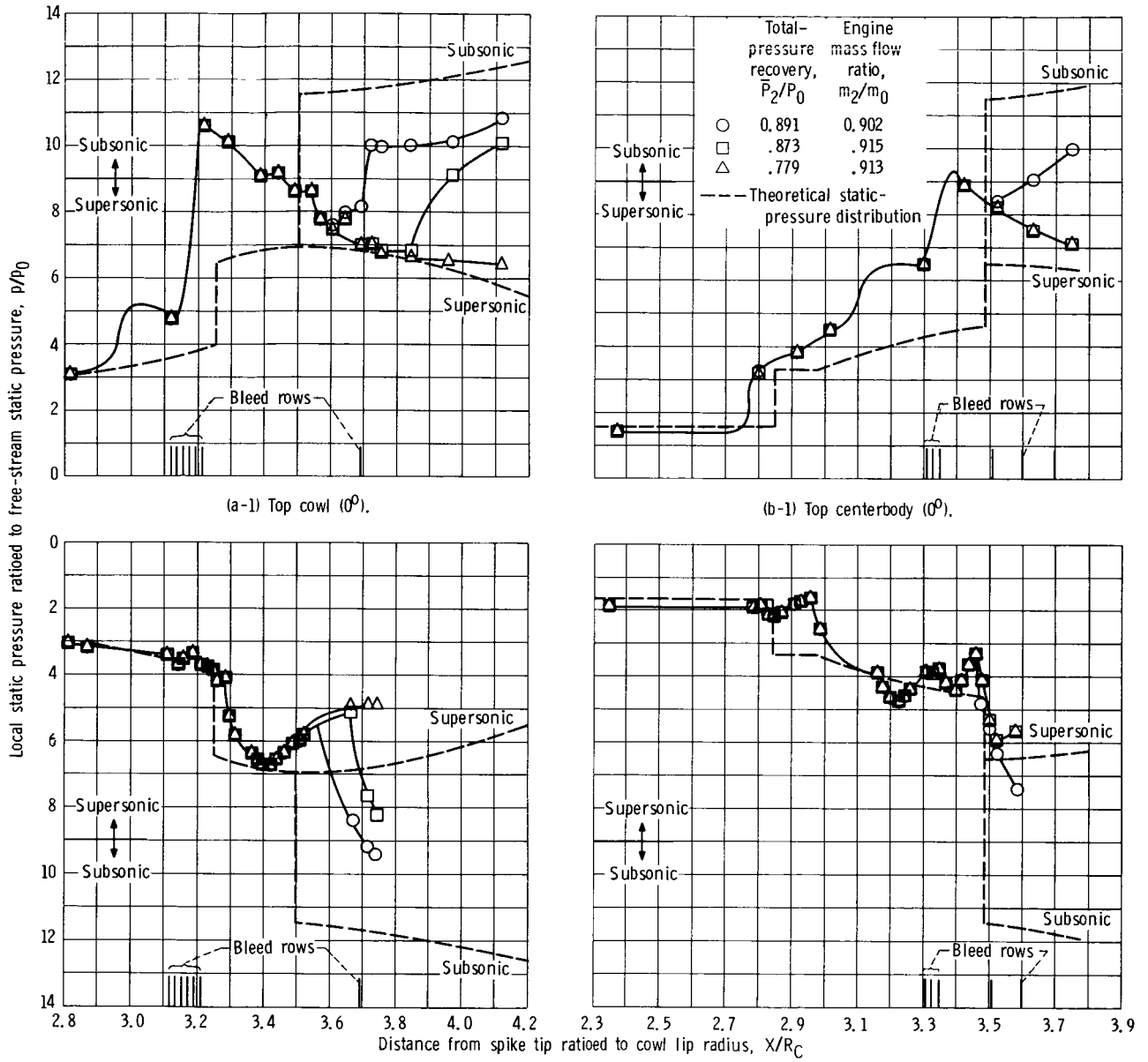

(a-1) Top cowl (0^0).

(b-1) Top centerbody (0^0).

(a-2) Bottom cowl (180^0).

(b-2) Bottom centerbody (180^0).

(a) Cowl surface; $M_0 = 2.495$; $\alpha = 3.8$

(b) Centerbody surface; $M_0 = 2.495$; $\alpha = 3.8^0$.

Figure 27. - Static-pressure distributions of 40-60 inlet at various operating limits for upstream bleed configuration. Cowl-lip-position parameter, 26.60^0.

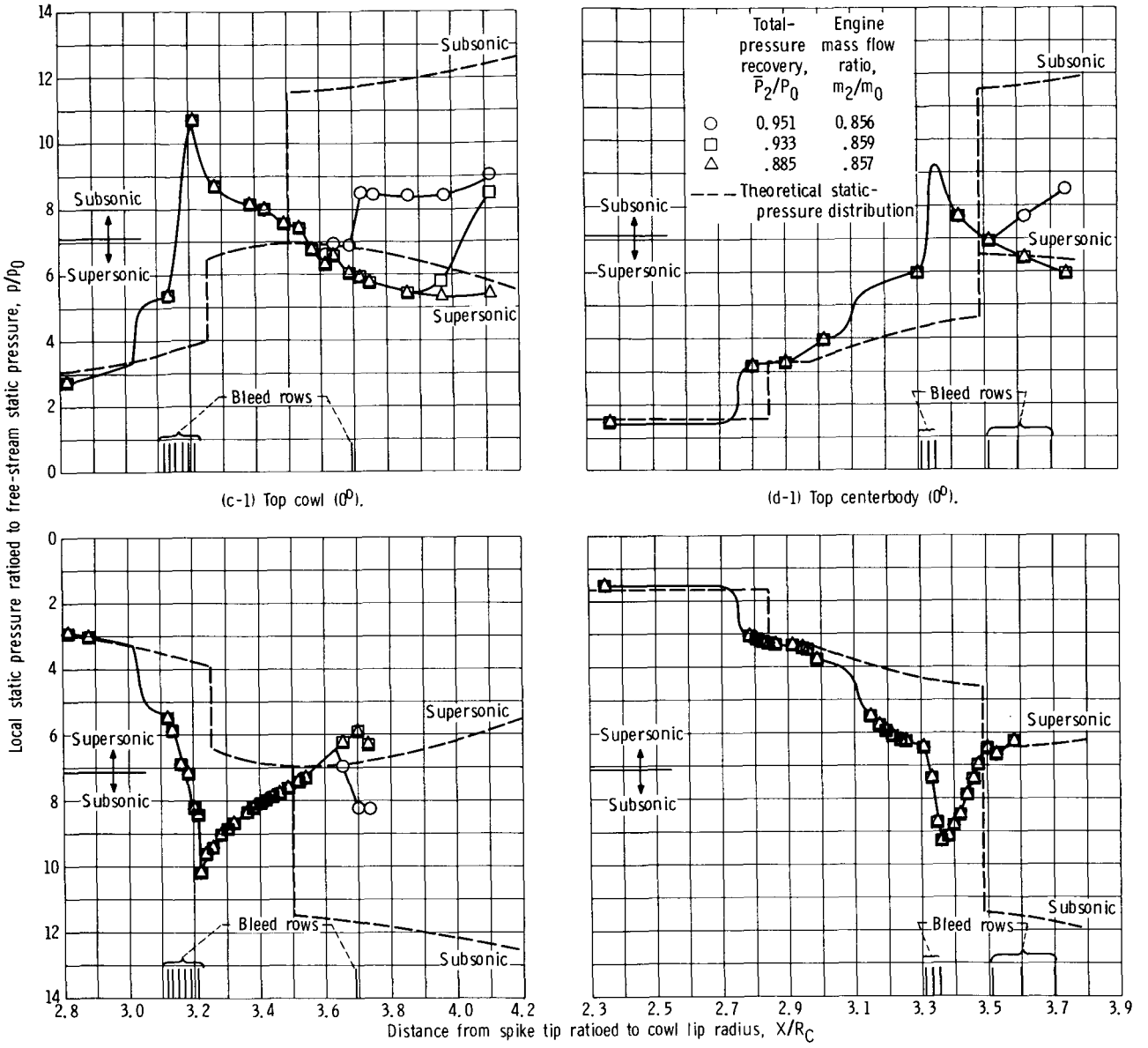

(c-1) Top cowl (0^0).

(d-1) Top centerbody (0^0).

(c-2) Bottom cowl (180^0).

(d-2) Bottom centerbody (180^0).

(c) Cowl surface; $M_0 = 2.345$; $\alpha = 0.10^0$.

(d) Centerbody surface; $M_0 = 2.345$; $\alpha = 0.10^0$.

Figure 27. - Concluded.

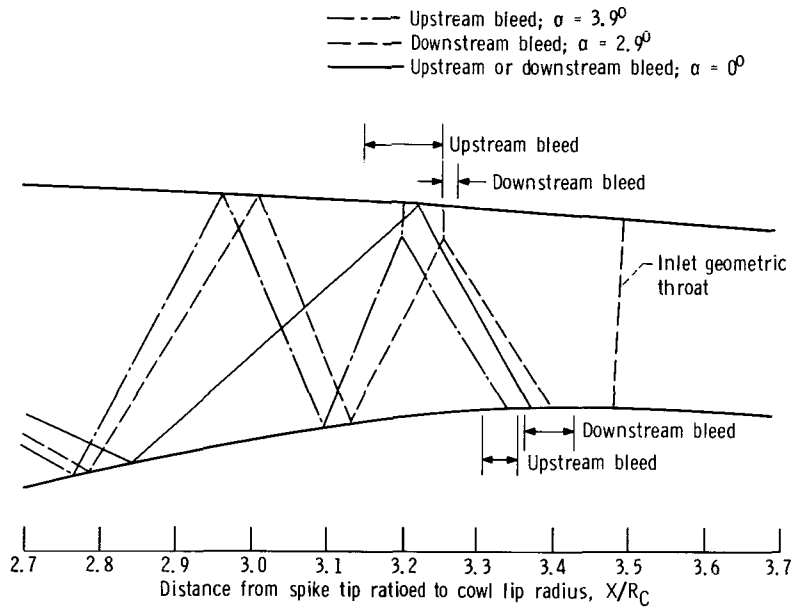

Figure 28. - Shock structures corresponding to maximum angle of attack operation for the upstream and downstream bleed configurations of 40-60 inlet. Cowl-lip-position parameter, 26.60°.

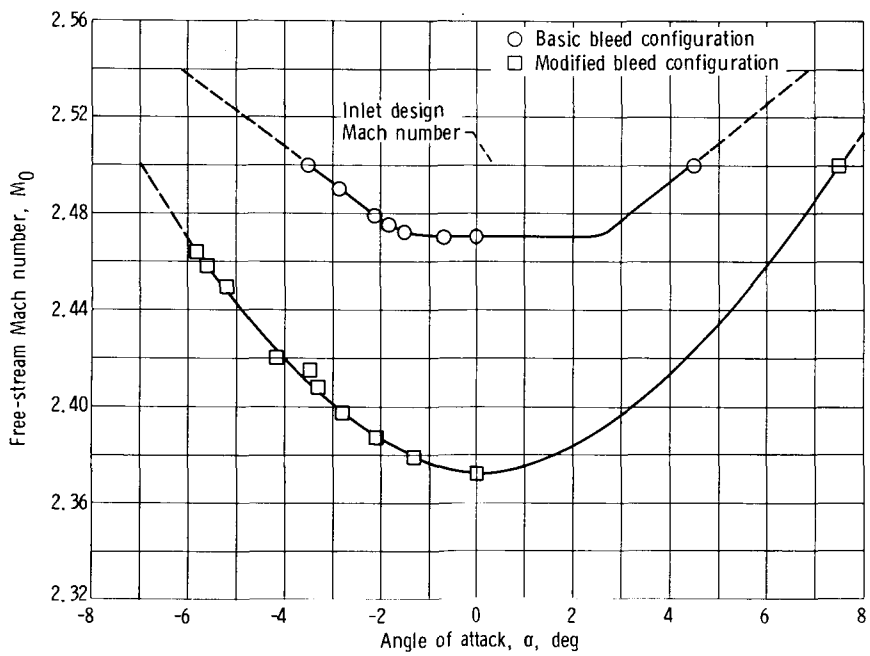

Figure 29. - Mach number - angle-of-attack characteristics of the 60-40 inlet with basic and modified bleed configurations. Cowl-lip-position parameter, 25.25°.

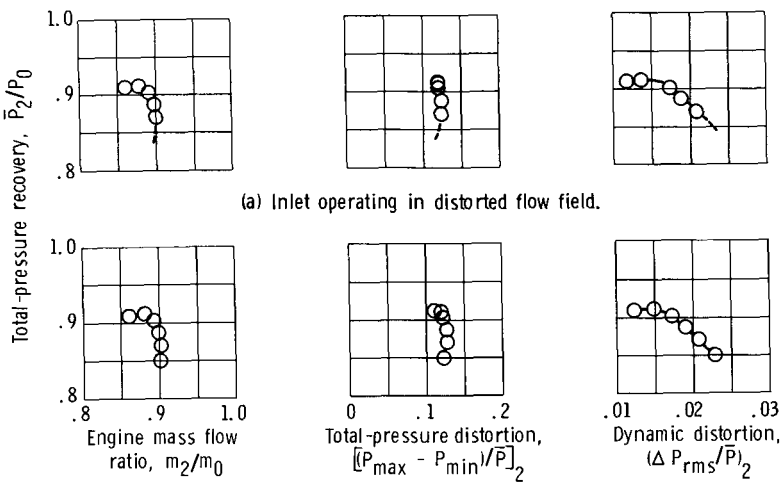

Figure 30. - Effect of flow field distortion on performance of 40-60 inlet with upstream bleed configuration. Cowl-lip-position parameter, 26.60^0.

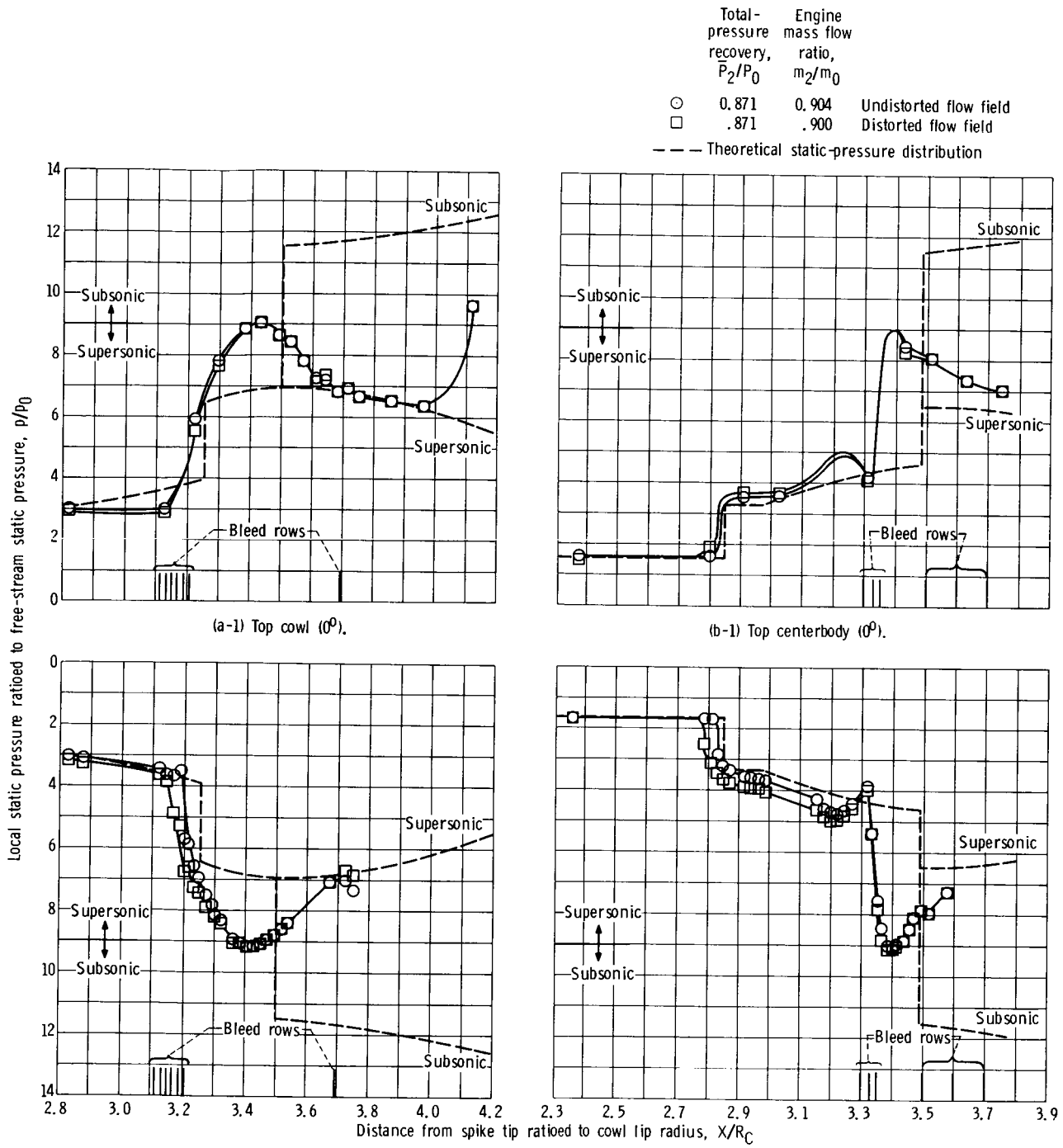

Figure 31. - Effect of flow field distortion on static-pressure distributions of 40-60 inlet with upstream bleed and 0° angle of attack. Cowl-lip-position parameter, 26.60°.

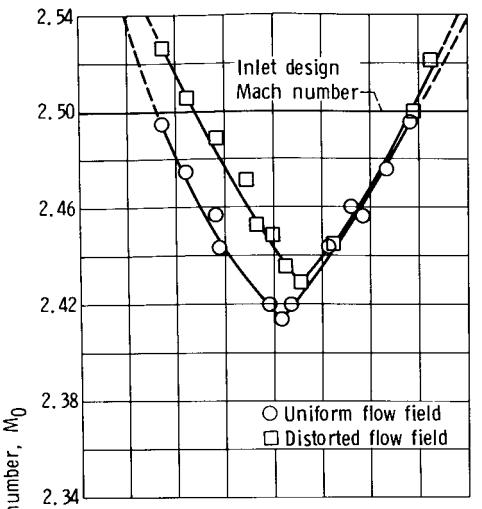

(a) Downstream bleed configuration.

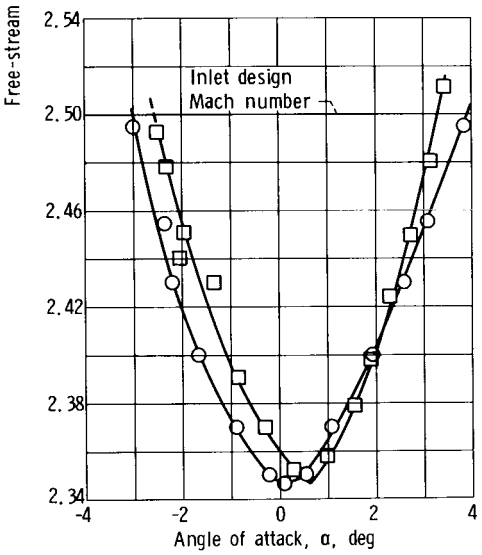

(b) Upstream bleed configuration.

Figure 32. - Effect of flow field distortion on tolerance of 40-60 inlet to changes in angle of attack and free-stream Mach number. Cowl-lip-position parameter, 26.60^0.

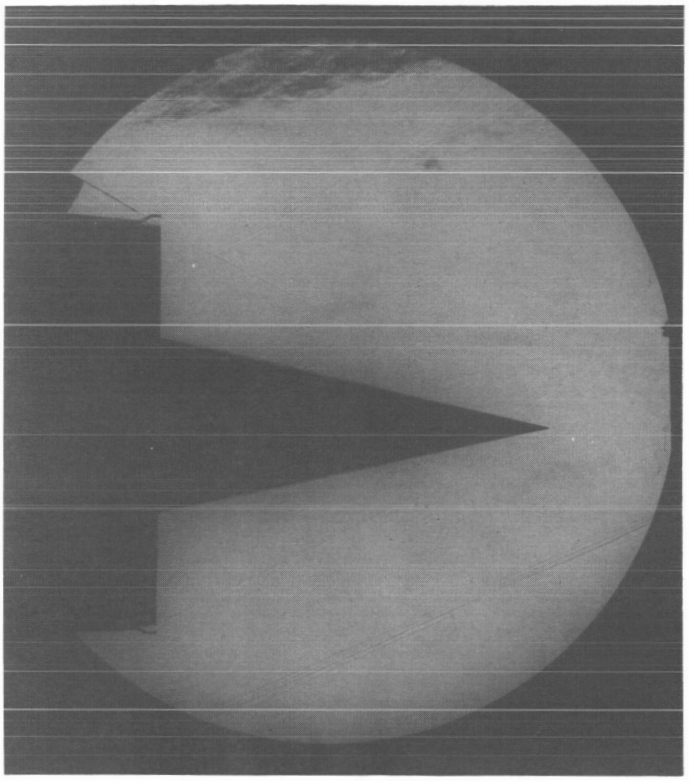

(a) $M = 2.50$; $\alpha = 0°$.

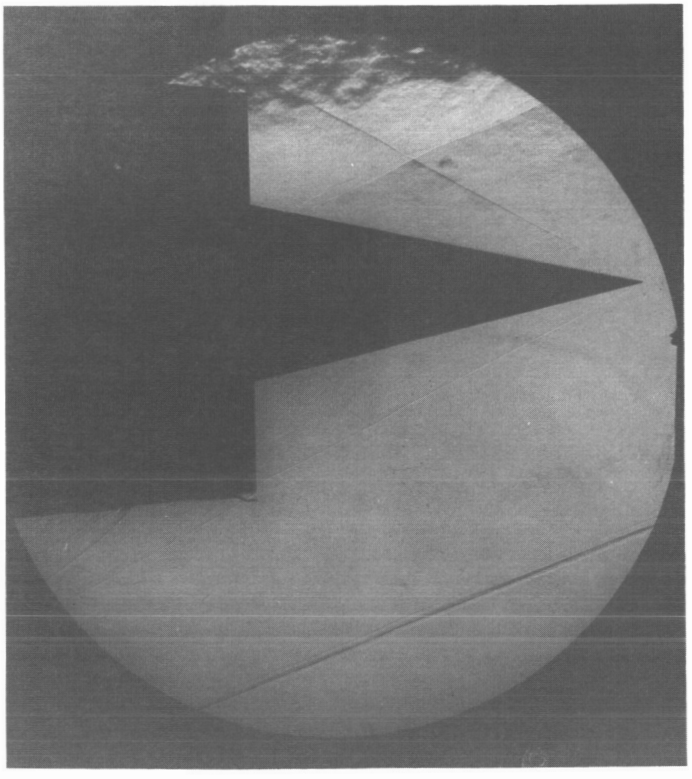

(b) $M = 2.50$; $\alpha = 3.8°$.

Figure 33. - Schlieren photographs of 40-60 inlet.

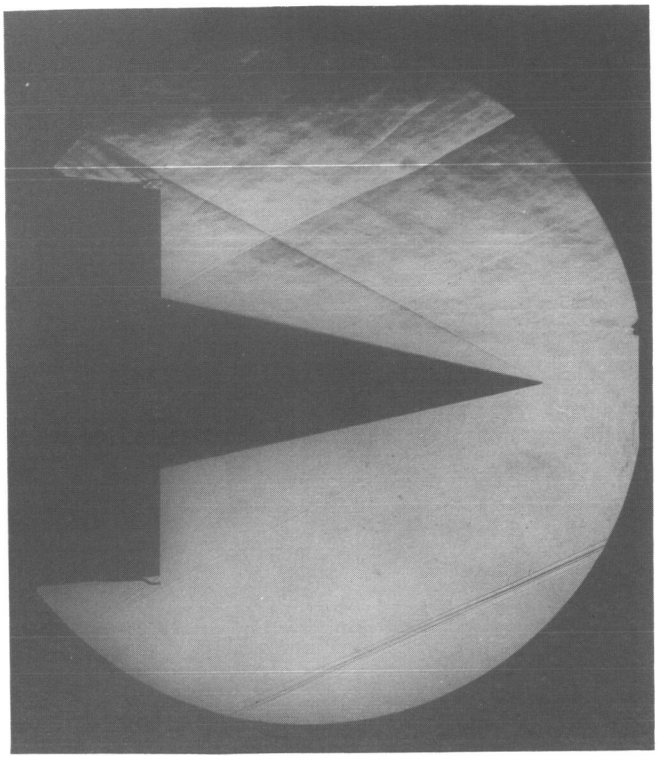

(c) $M = 2.34$; $\alpha = 0.10°$.

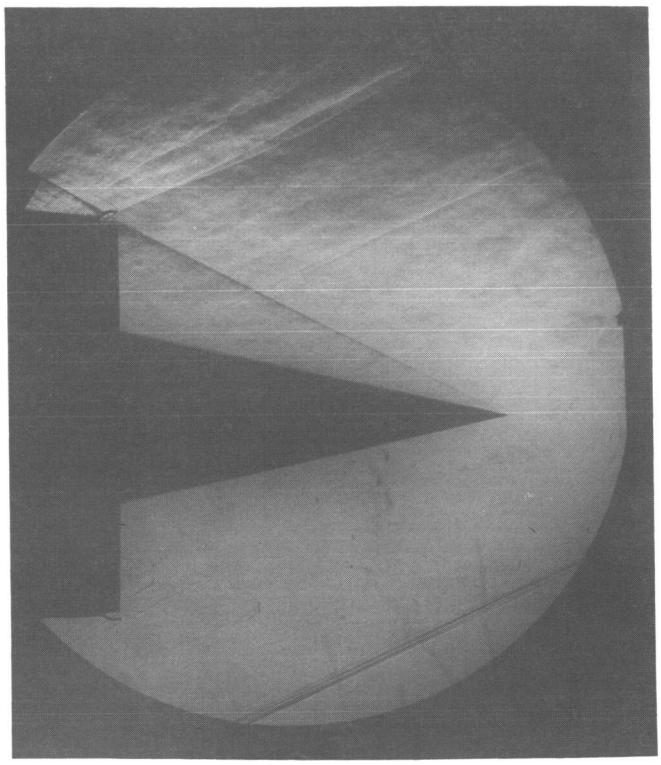

(d) $\overline{M} = 2.5$; $\overline{\alpha} = 0°$.

Figure 33. - Continued.

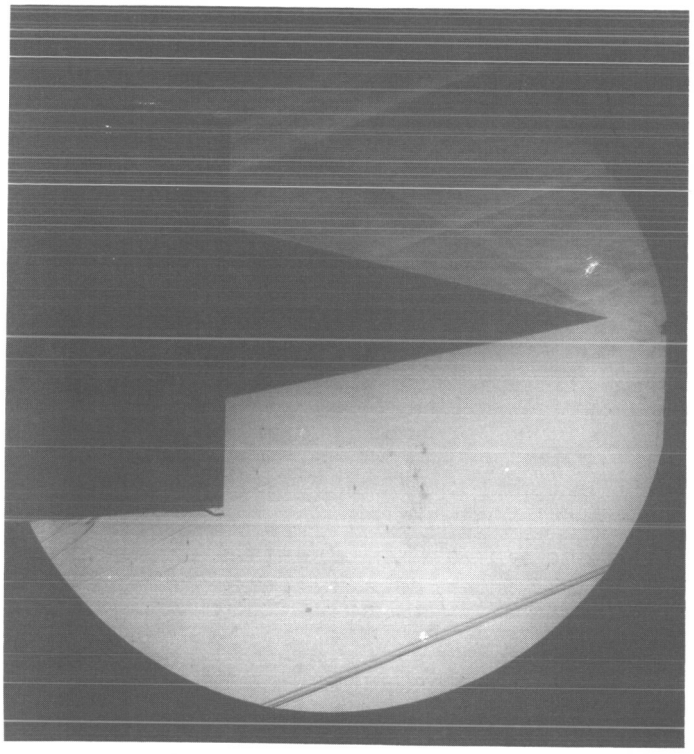

(e) $\overline{M} = 2.50$; $\overline{\alpha} = 2.91°$.

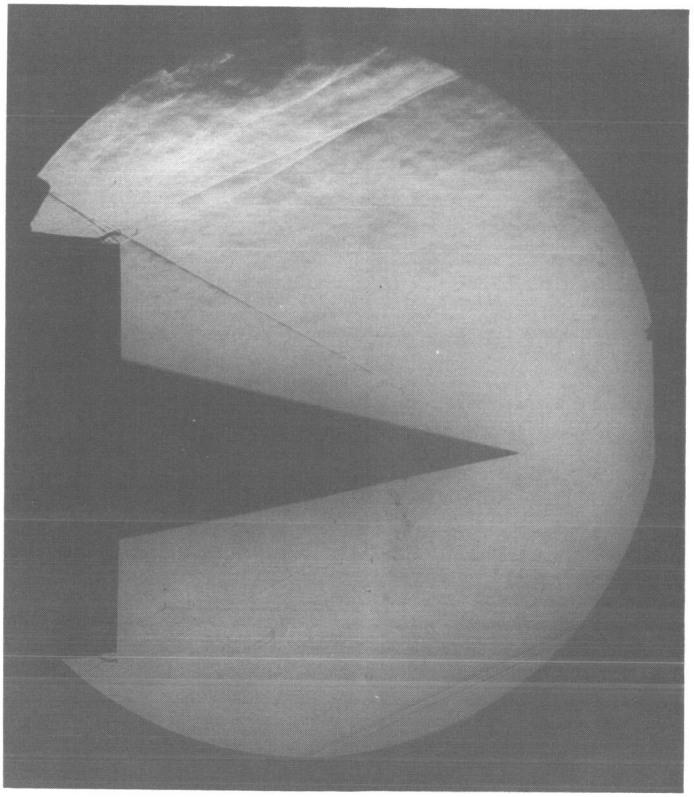

(f) $\overline{M} = 2.43$; $\overline{\alpha} = 0.55°$.

Figure 33. - Concluded.

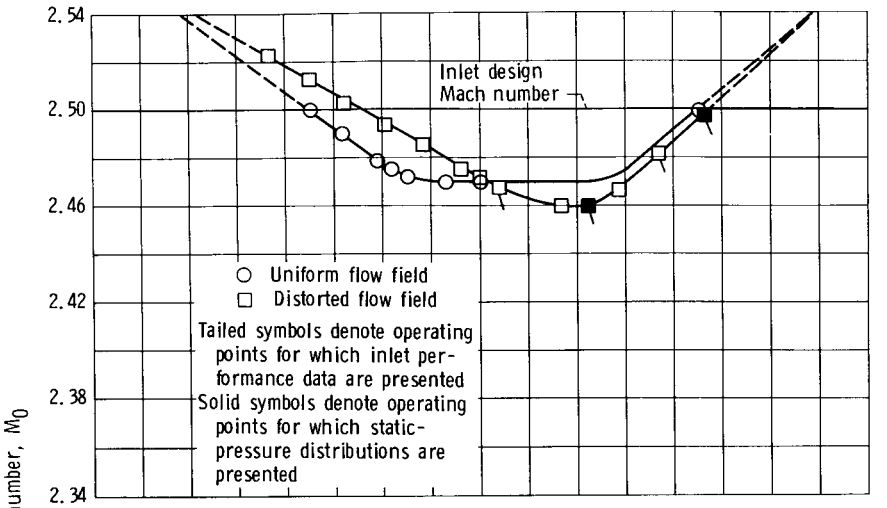

(a) Basic bleed configuration.

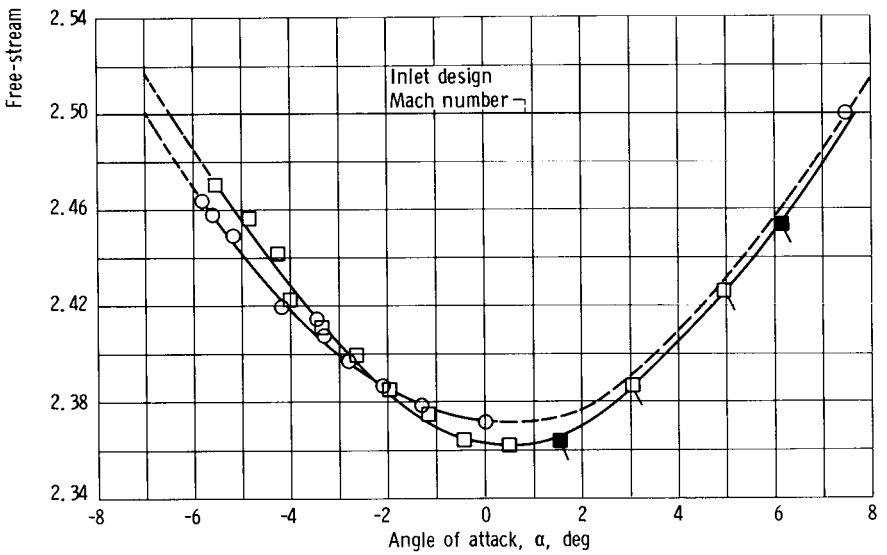

(b) Modified bleed configuration.

Figure 34. - Effect of flow field distortion on Mach number - angle-of-attack tolerance for 60-40 inlet. Cowl-lip-position parameter, 25.25°.

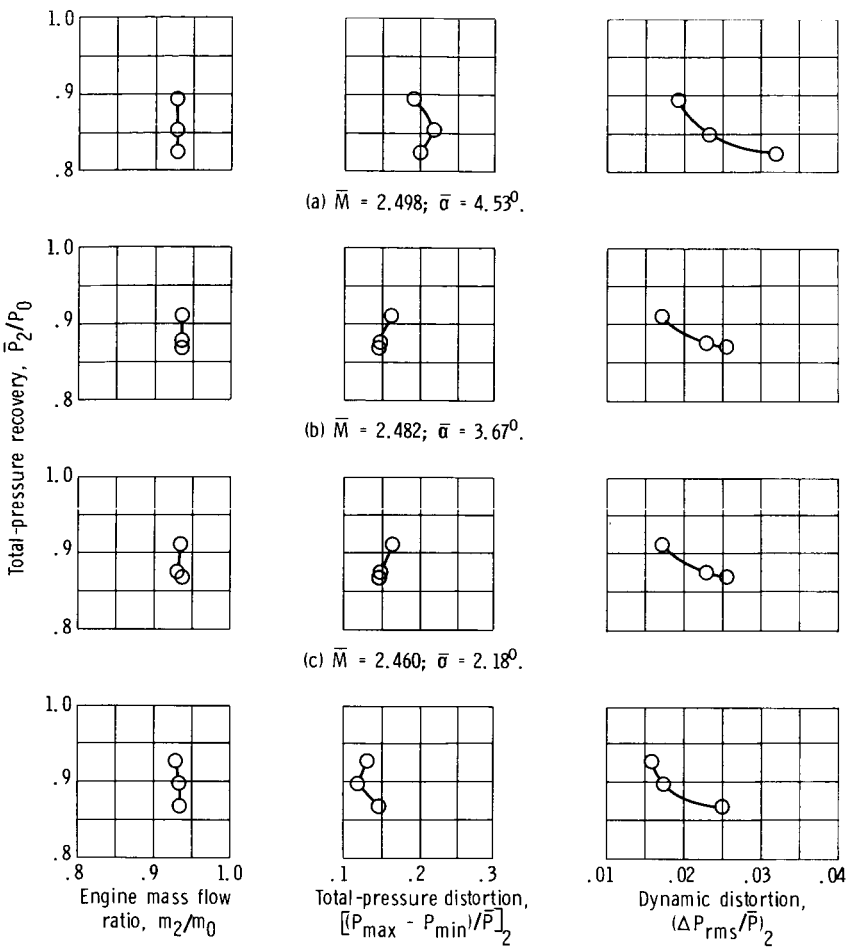

Figure 35. - Performance of 60-40 inlet at various limits for basic bleed configuration. Cowl-lip-position parameter, 25.25°.

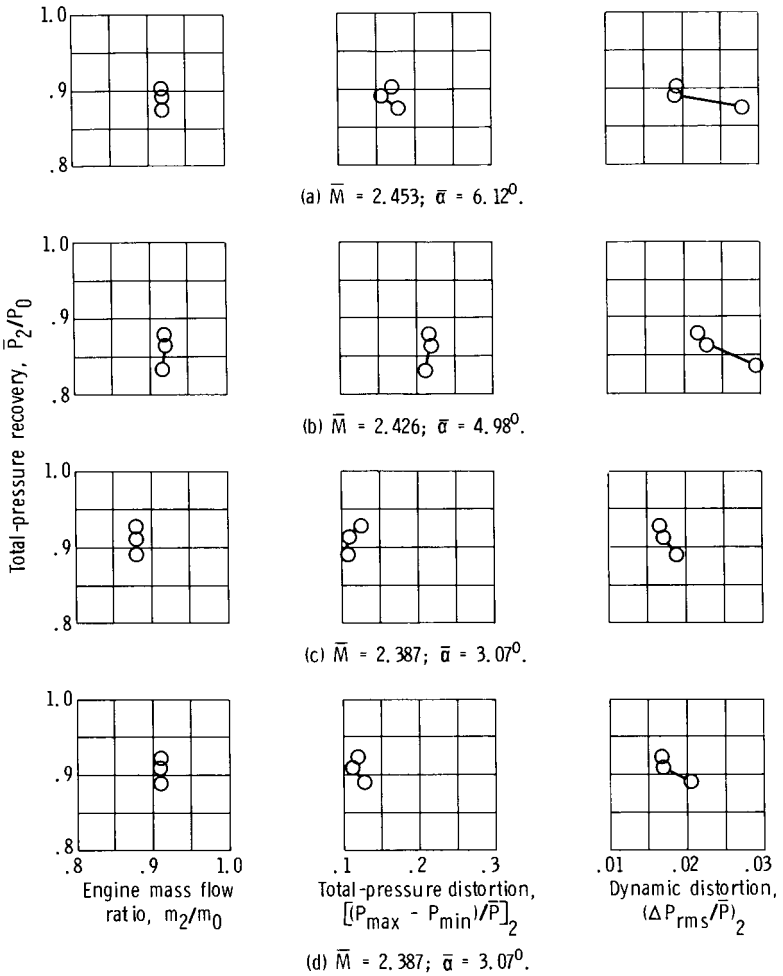

Figure 36. - Performance of 60-40 inlet at various limits for modified bleed configuration. Cowl-lip-position parameter, 25.25°.

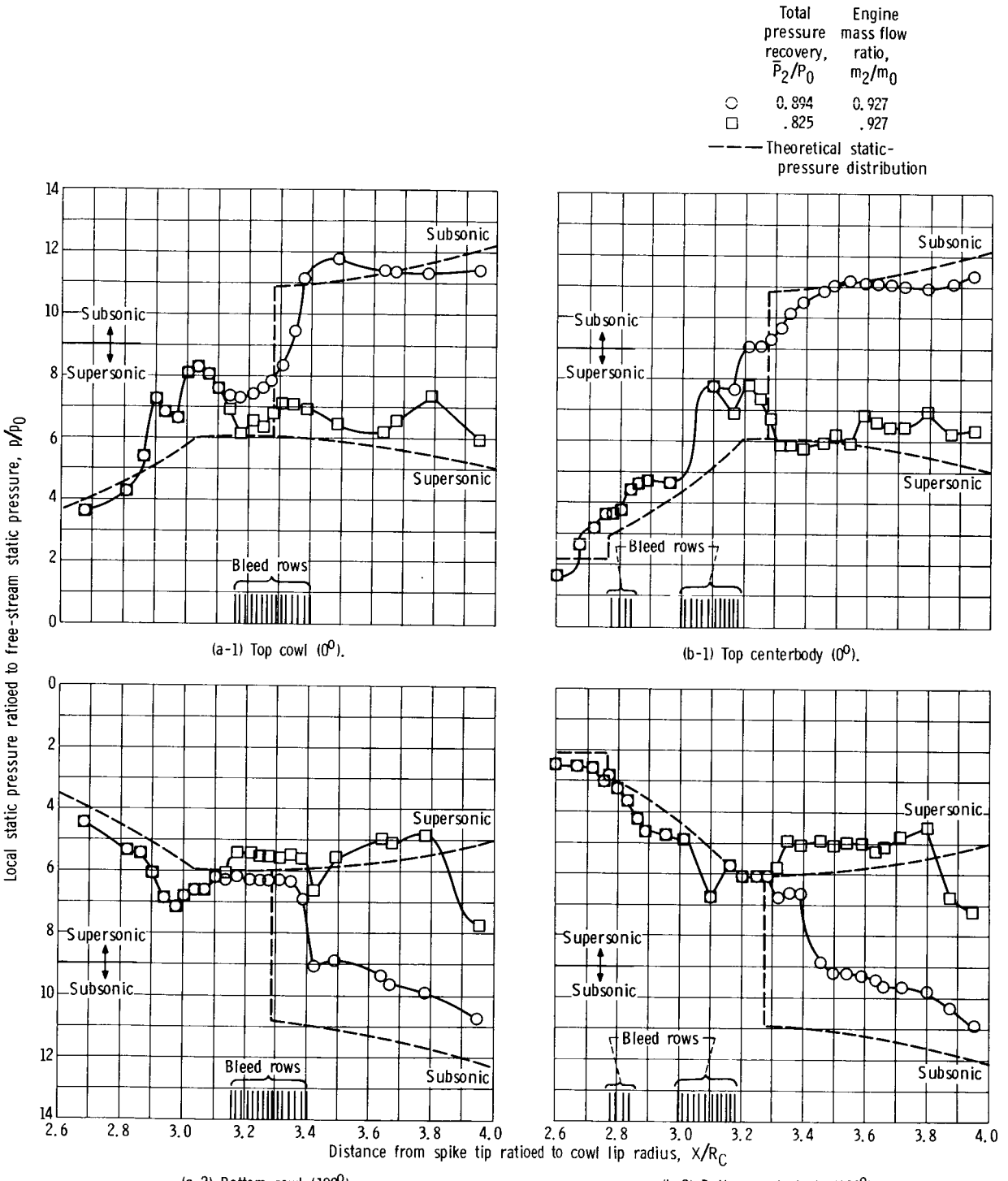

(a) Cowl surface; $\bar{M}$ = 2.498; $\bar{\alpha}$ = 4.53°.

(b) Centerbody surface; $\bar{M}$ = 2.498; $\bar{\alpha}$ = 4.53°.

Figure 37. - Static-pressure distributions of 60-40 inlet at various operating limits for basic bleed configuration. Cowl-lip-position parameter, 25.25°.

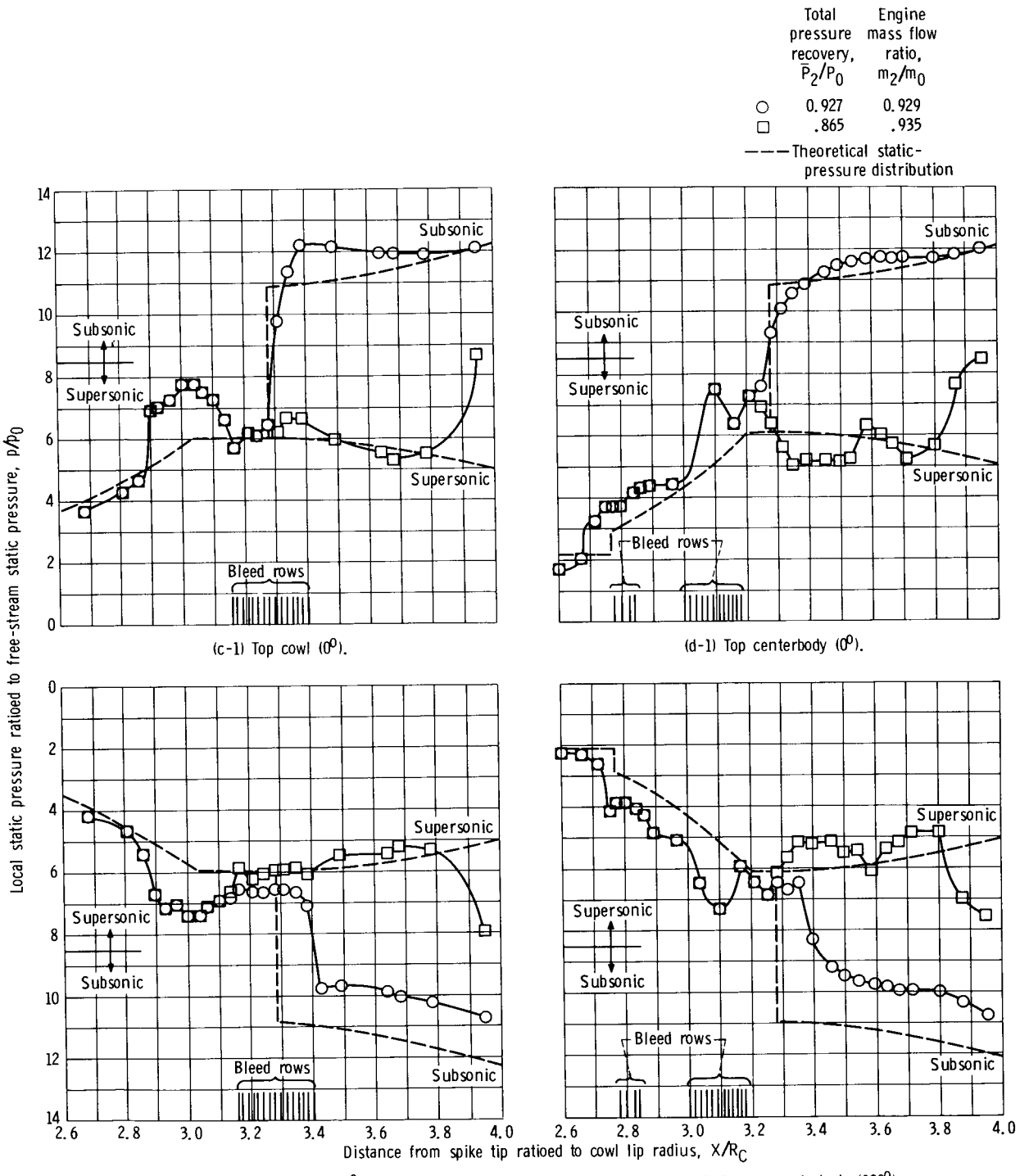

(c-1) Top cowl (0^0).

(d-1) Top centerbody (0^0).

(c-2) Bottom cowl (180^0).

(d-2) Bottom centerbody (180^0).

(c) Cowl surface; $\bar{M} = 2.460$; $\bar{\alpha} = 2.18^0$.

(d) Centerbody surface; $\bar{M} = 2.460$; $\bar{\alpha} = 2.18^0$.

Figure 37. - Concluded.

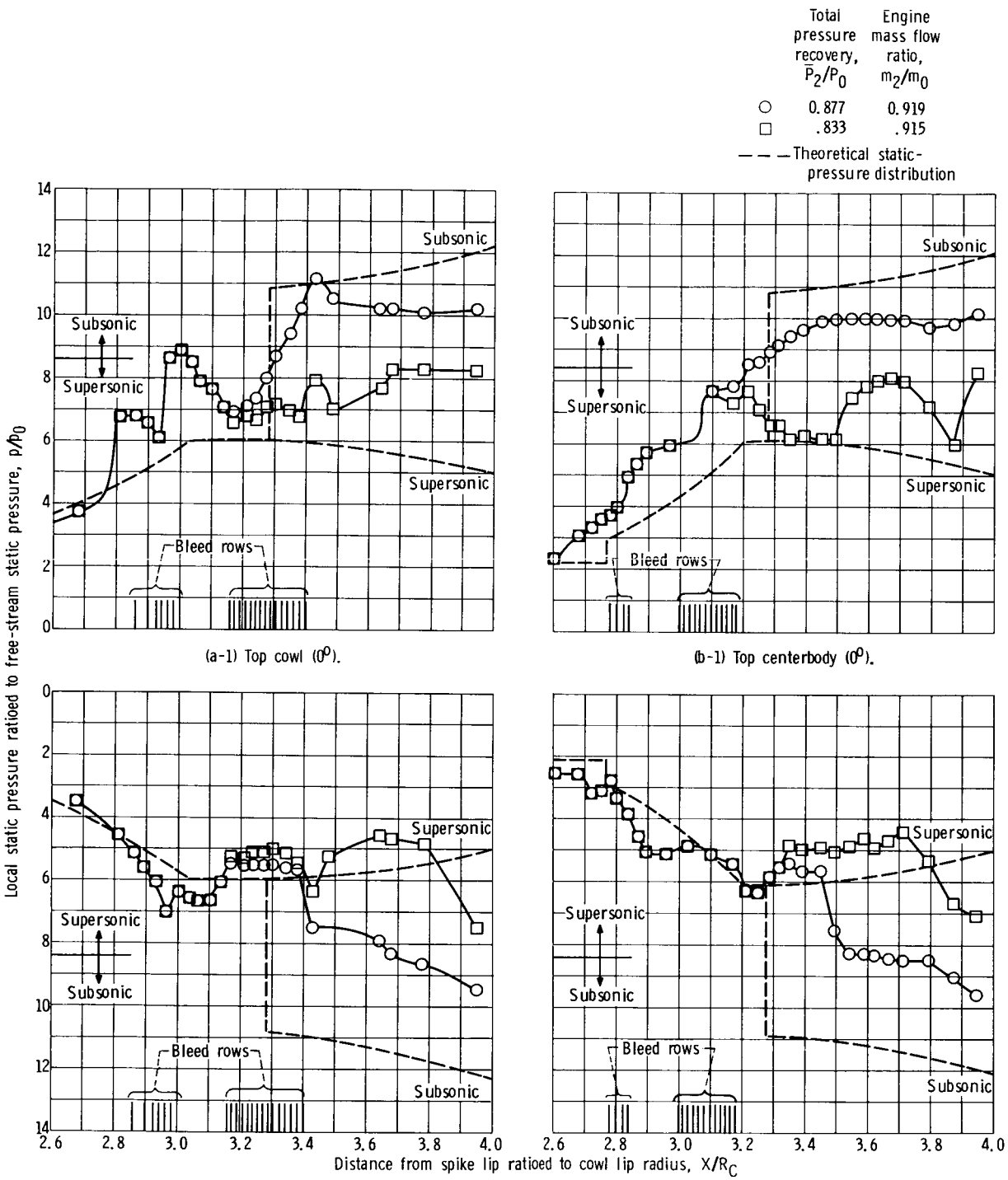

(a-1) Top cowl (0^0).

(b-1) Top centerbody (0^0).

(a-2) Bottom cowl (180^0).

(b-2) Bottom centerbody (180^0).

(a) Cowl surface; $\bar{M} = 2.453$; $\bar{\alpha} = 6.12^0$.

(b) Centerbody surface; $\bar{M} = 2.453$; $\bar{\alpha} = 6.12^0$.

Figure 38. - Static-pressure distributions of 60-40 inlet at various operating limits for modified bleed configuration. Cowl-lip-position parameter, 25.25^0.

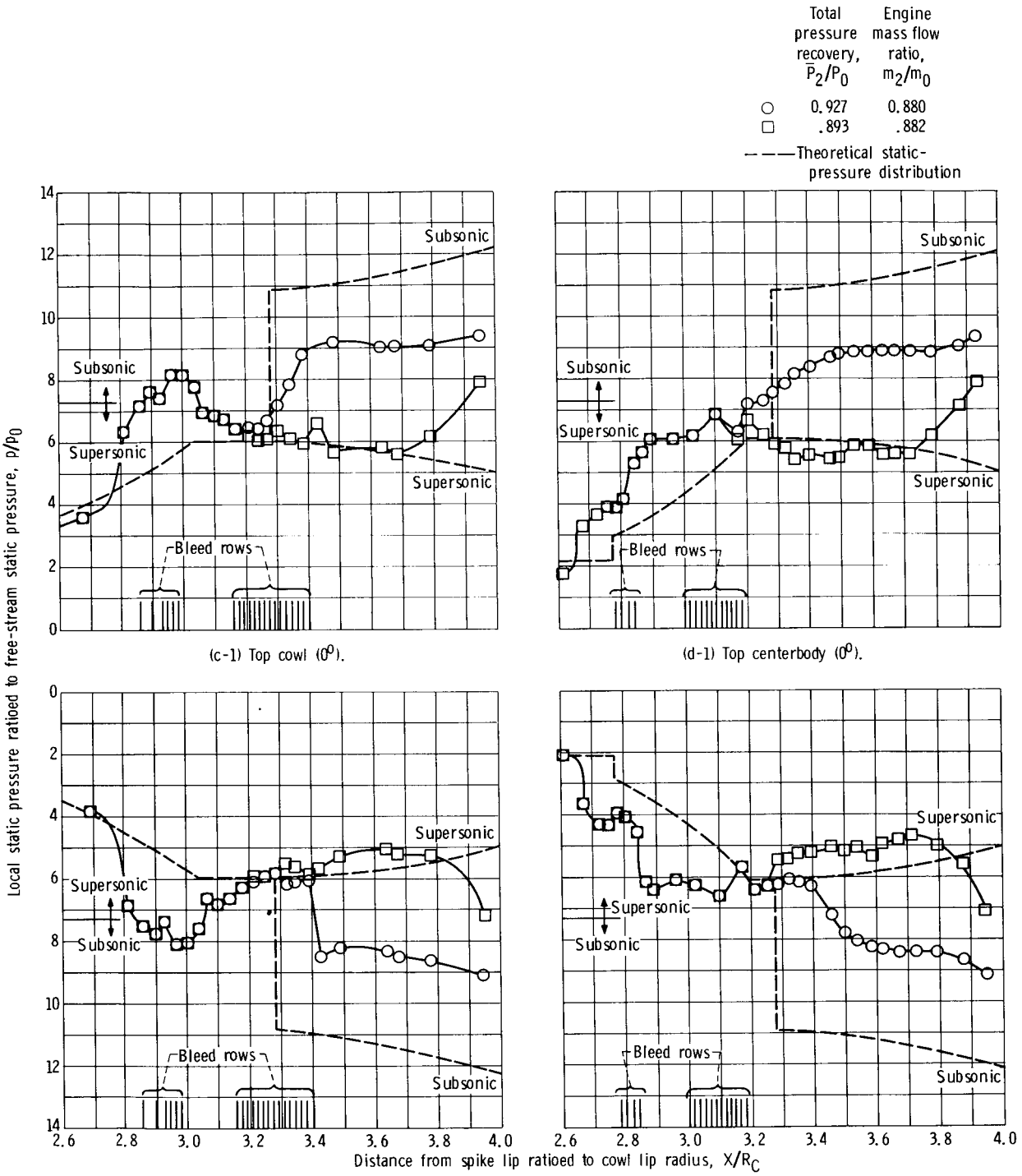

(c-1) Top cowl (0^0).

(d-1) Top centerbody (0^0).

(c-2) Bottom cowl (180^0).

(d-2) Bottom centerbody (180^0).

(c) Cowl surface; $\bar{M} = 2.364$; $\bar{\alpha} = 1.53^0$.

(d) Centerbody surface; $\bar{M} = 2.364$; $\bar{\alpha} = 1.53^0$.

Figure 38. - Concluded.